INQNET Internal Physics Notes

Samantha I Davis

June 28, 2021

Contents

Chapter 1

Teleportation Systems Towards a Quantum Internet

1.1 Introduction

Quantum teleportation is essential to many architectures of long-distance quantum networks, which are expected to form part of a future quantum internet. Here we present a semi-automated quantum teleportation system capable of teleporting time-bin qubits at a telecommunication wavelength of 1536.5 nm with $\sim$ 90% fidelities over 45km of optical fiber spools. Our systems use commercially available fiber optics, which enable straightforward implementation and flexibility, and state-of- the-art superconducting nanowire single photon detectors (SNSPDs). Our system [16] will serve as the basis for a quantum network with nodes at Caltech and Fermilab, a step towards a prototype for a quantum internet connecting the 17 US national labs.

Quantum Teleportation for Quantum Networks

Quantum cryptographic protocols such as quantum teleportation are promising candidates for virtually unhackable modes of communication due to their sensitivity to eavesdroppers. This motivates the construction of networks of quantum channels ("quantum networks") to not only enable quantum-secure communications, but also form part of a "quantum internet": a globally-distributed set of quantum processers and sensors connected by a network that can allocate quantum resources (e.g. qubits and entangled states) across different nodes. [20]

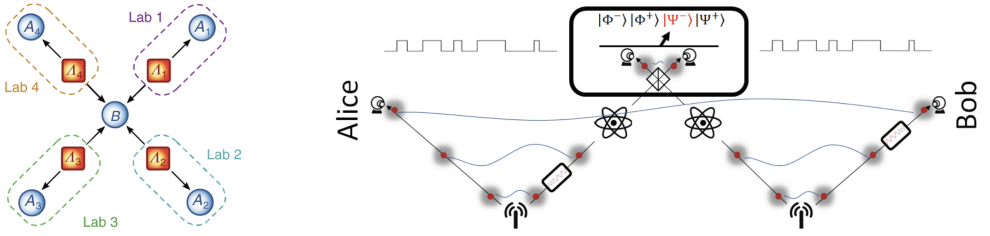

(a) Star-like quantum network [14]

(b) Quantum repeater architecture for entanglement swapping [1]

Figure 1.1: Quantum network architectures

Many architectures for quantum networks, such as star-type networks and quantum repeaters (Figure 1.2), require quantum teleportation to overcome the significant rate and loss limitations of the direct transmission of qubits. As such, it is desirable to develop high-fidelity teleportation systems using commercially available components that are compatible with emerging quantum devices and allow straightforward replication and deployment of quantum networks.

One approach to building large-scale quantum networks is to leverage the optical fiber networks that are already deployed for classical communications. For this approach, qubits encoded in the time-of-arrival states (early $|e\rangle$ or late $|\ell\rangle$) of individual photons, or time-bin qubits, at telecom-band wavelengths

are preferred due to their ease of generation, ability to propagate over long distances in fiber, and robustness to the dynamics of the real world.

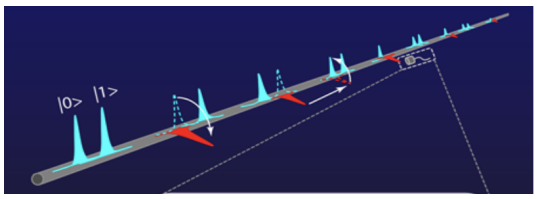

(a) Conceptual diagram of time-bin qubits propagating through optical fiber [12]

(b) Artistic depiction of fiber optic quantum network [13]

Figure 1.2: Quantum network architectures

1.2 Quantum Teleportation Protocol

The quantum teleportation protocol enables users to securely send and receive messages encoded in quantum states.

Alice wants to send a quantum state $|\psi\rangle = \alpha|0\rangle + \beta e^{i\phi}|1\rangle$ to Bob. To do this, Alice prepares time-bin qubit (A) in state $|\psi_A\rangle = \alpha|e\rangle_A + \beta e^{i\phi}|\ell\rangle_A$ with $|\alpha|^2 + |\beta|^2 = 1$ and sends her qubit to a third party, Charlie, who is position between Alice and Bob. Bob creates an entangled pair of time-bin qubits (B,B') in state $\frac{1}{\sqrt{2}}(|e\rangle_B|e\rangle_{B'} + |\ell\rangle_B|\ell\rangle_{B'})$ and sends qubit B' to Charlie.

The full state of the system is

$$|\psi\rangle_{sys} = \frac{1}{\sqrt{2}}|\psi\rangle_A \otimes (|e\rangle_B|e\rangle_{B'} + |\ell\rangle_B|\ell\rangle_{B'}) = \frac{1}{\sqrt{2}}(\alpha|e\rangle_A + \beta e^{i\phi}|\ell\rangle_A) \otimes (|e\rangle_B|e\rangle_{B'} + |\ell\rangle_B|\ell\rangle_{B'}) \quad (1.1)$$

By expanding $|\psi\rangle_{sys}$ as

$$|\psi\rangle_{sys} = \frac{1}{\sqrt{2}}(\alpha|e\rangle_A|e\rangle_B|e\rangle_{B'} + \alpha|e\rangle_A|\ell\rangle_B|\ell\rangle_{B'} + \beta e^{i\phi}|\ell\rangle_A|e\rangle_B|e\rangle_{B'} + \beta e^{i\phi}|\ell\rangle_A|\ell\rangle_B|\ell\rangle_{B'}) \quad (1.2)$$

we see that we can re-express $|\psi\rangle_{sys}$ in terms of Bell States,

$$|\Phi^+\rangle_{AB} = \frac{1}{\sqrt{2}}(|e\rangle_A|e\rangle_B + |\ell\rangle_A|\ell\rangle_B) \quad (1.3)$$

$$|\Phi^-\rangle_{AB} = \frac{1}{\sqrt{2}}(|e\rangle_A|e\rangle_B - |\ell\rangle_A|\ell\rangle_B) \quad (1.4)$$

$$|\Psi^+\rangle_{AB} = \frac{1}{\sqrt{2}}(|e\rangle_A|\ell\rangle_B + |\ell\rangle_A|e\rangle_B) \quad (1.5)$$

$$|\Psi^-\rangle_{AB} = \frac{1}{\sqrt{2}}(|e\rangle_A|\ell\rangle_B - |\ell\rangle_A|e\rangle_B) \quad (1.6)$$

with the following substitutions:

$$\frac{1}{\sqrt{2}}(|e\rangle_A|e\rangle_B) = \frac{1}{2}(|\Phi^+\rangle_{AB} + |\Phi^-\rangle_{AB}) \quad (1.7)$$

$$\frac{1}{\sqrt{2}}(|\ell\rangle_A|\ell\rangle_B) = \frac{1}{2}(|\Phi^+\rangle_{AB} - |\Phi^-\rangle_{AB}) \quad (1.8)$$

$$\frac{1}{\sqrt{2}}(|e\rangle_A|\ell\rangle_B) = \frac{1}{2}(|\Psi^+\rangle_{AB} + |\Psi^-\rangle_{AB}) \quad (1.9)$$

$$\frac{1}{\sqrt{2}}(|\ell\rangle_A|e\rangle_B) = \frac{1}{2}(|\Psi^+\rangle_{AB} - |\Psi^-\rangle_{AB}) \quad (1.10)$$

Substituting and rearranging terms,

$$|\psi\rangle_{sys} = \frac{1}{2}\big(\alpha(|\Phi^+\rangle_{AB} + |\Phi^-\rangle_{AB})\,|e\rangle_{B'} + \alpha(|\Psi^+\rangle_{AB} + |\Psi^-\rangle_{AB})\,|\ell\rangle_{B'} + \beta e^{i\phi}(|\Psi^+\rangle_{AB} - |\Psi^-\rangle_{AB})\,|e\rangle_{B'} + \beta e^{i\phi}(|\Phi^+\rangle_{AB} - |\Phi^-\rangle_{AB})\,|\ell\rangle_{B'}\big) \tag{1.11}$$

$$|\psi\rangle_{sys} = \frac{1}{2}\big(|\Phi^+\rangle_{AB}(\alpha\,|e\rangle_{B'} + \beta e^{i\phi}\,|\ell\rangle_{B'}) + |\Phi^-\rangle_{AB}(\alpha\,|e\rangle_{B'} - \beta e^{i\phi}\,|\ell\rangle_{B'}) + |\Psi^+\rangle_{AB}(\alpha\,|\ell\rangle_{B'} + \beta e^{i\phi}\,|e\rangle_{B'}) + |\Psi^-\rangle_{AB}(\alpha\,|\ell\rangle_{B'} - \beta e^{i\phi}\,|e\rangle_{B'})\big) \tag{1.12}$$

Recall the purpose of this protocol: we want to send Alice's initial state, $|e\rangle_A + e^{i\phi}\,|\ell\rangle_A$ to Bob, who has qubit $|\psi_{B'}\rangle$. From equation (1.12), we see that if Charlie projects onto one of the four Bell states, Bob's qubit will occupy Alice's initial state, up to a unitary gate transformation.

$$\text{Projection onto } |\Phi^+\rangle_{AB} \Longleftrightarrow |\psi\rangle_{B'} = \alpha\,|e\rangle_{B'} + \beta e^{i\phi}\,|\ell\rangle_{B'} \rightarrow \text{Apply } \hat{\mathbb{I}} \text{ to } |\psi\rangle_{B'} \tag{1.13}$$

$$\text{Projection onto } |\Phi^-\rangle_{AB} \Longleftrightarrow |\psi\rangle_{B'} = \alpha\,|e\rangle_{B'} - \beta e^{i\phi}\,|\ell\rangle_{B'} \rightarrow \text{Apply } \hat{\sigma}_z \text{ to } |\psi\rangle_{B'} \tag{1.14}$$

$$\text{Projection onto } |\Psi^+\rangle_{AB} \Longleftrightarrow |\psi\rangle_{B'} = \alpha\,|\ell\rangle_{B'} + \beta e^{i\phi}\,|e\rangle_{B'} \rightarrow \text{Apply } \hat{\sigma}_x \text{ to } |\psi\rangle_{B'} \tag{1.15}$$

$$\text{Projection onto } |\Psi^-\rangle_{AB} \Longleftrightarrow |\psi\rangle_{B'} = \alpha\,|\ell\rangle_{B'} - \beta e^{i\phi}\,|e\rangle_{B'} \rightarrow \text{Apply } \hat{\sigma}_x\hat{\sigma}_z \text{ to } |\psi\rangle_{B'} \tag{1.16}$$

Charlie (classically) communicates the result of his Bell State measurement to Bob, who then knows what gate to apply to his qubit to retrieve Alice's initial state. If Charlie projected onto $|\Phi^+\rangle_{AB}$, Bob applies the identity gate (or does nothing) to his qubit, if Charlie projected onto $|\Phi^-\rangle_{AB}$, Bob applies the Pauli-X gate to his qubit, if Charlie projected onto $|\Psi^+\rangle_{AB}$, Bob applies the Pauli-Z (R_π) to his qubit, and if Charlie projected onto $|\Psi^-\rangle_{AB}$, Bob applies the Pauli-Z then Pauli-X gates to his qubit.

1.2.1 Experiment

We have built a teleportation network modeled after the midpoint configuration of the quantum repeater protocol using off-the-shelf fiber optic components. In our configuration, a third agent (Charlie) is introduced between Alice and Bob to perform the Bell State measurement, and the entanglement source is at Bob. State-of-the-art superconducting single photon detectors (SNSPDs) are used to project onto the Bell State basis at Charlie and measure the teleported states at Bob.

The experimental set-up is depicted in Figure 1.3. Time-bin qubit states at telecommunication wavelength are prepared by injecting pulses from an arbitrary wave generator into 1536nm (coherent) laser light at 90MHz using high extinction ratio intensity modulators (IM) at Alice and Bob. To produce $|e\rangle$ and $|l\rangle$, a single pulse is injected per clock cycle (where $|l\rangle$ has a 2ns delay relative to $|e\rangle$), and to produce superposition states $|e\rangle^{i\phi}\,|l\rangle$, two pulses separated by 2ns are injected per clock cycle.

Alice: Single Qubit Generation

Following the protocol, Alice prepares a qubit in state $\alpha\,|e\rangle + \beta e^{i\phi}\,|l\rangle$. After Alice prepares the state of her qubit (qubit A), the coherent light from Alice is filtered by a 30GHz bandwidth Fiber Bragg Grating (FBG) with a central wavelength of 1536.49 nm and attenuated to the single photon level with a variable optical attenuator (VOA). Before reaching Charlie, the light from Alice passes through a polarization controller (POC) and 22km of fiber spool (FIS).

Bob: Entanglement Generation and Teleported-Qubit Measurement

Bob creates pairs of entangled photons with state $\frac{1}{\sqrt{2}}(|e\rangle \otimes |l\rangle_{B'} + |l\rangle_B \otimes |e\rangle_{B'})$ by preparing light in state $|e\rangle + |l\rangle$, amplifying the light with an erbium doped fiber amplifier (EDFA), and then pumping the light into a second harmonic generation (SHG) nonlinear crystal followed by a type II spontaneous parametric downconversion (SPDC) nonlinear crystal. At the output of SPDC, Bob uses a polarizing beamsplitter (PBS) followed by an FBG, a POC, and 11km of fiber spool to split the entangled photon

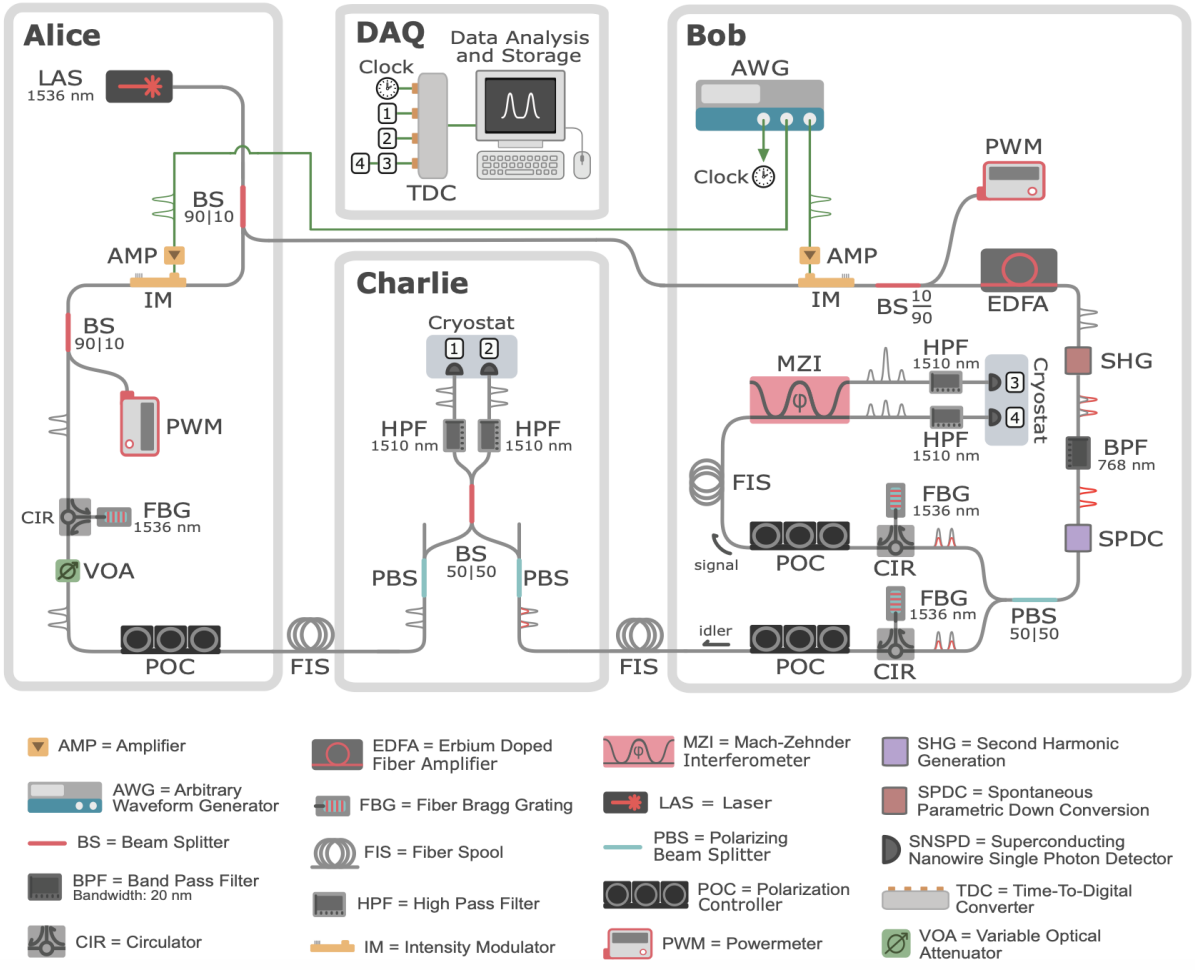

Figure 1.3: Teleportation System Experimental Setup

pairs. One member of each entangled pair (qubit B) stays at Bob and enters an unbalanced Mach-Zehnder interferometer (MZI) with a relative 2ns path latency. The outputs of the MZI are connected to high pass filters and detectors (3 and 4). The qubit phase factor $e^{i\phi}$ determined by tuning the phase A of the MZI and measuring the resulting interference pattern with detectors 3 and 4. This enables Bob to characterize the state of qubit and verify the success of teleportation.

Charlie: Bell State Measurement

The other member of the entangled pair (qubit C) is sent to Charlie. Charlie uses a 50:50 beamsplitter to project qubits A and C onto the Bell state basis. At each beamsplitter output, high pass filters (HPF) in series with detectors (1 and 2) are used to block vestigial pump light and measure the state of qubits. In particular, projection onto $|\Psi^-\rangle_{AB'}$ is achieved by measuring coincidences of $|e\rangle_A$ at detector 1 and $|l\rangle_{B'}$ at detector 2 or $|l\rangle_A$ at detector 1 and $|l\rangle_{B'}$ at detector 2 .

1.2.2 Data Acquisition, Storage, and Analysis

We have developed software to remotely store, analyze, and monitor data in real time. The SNSPDs at Bob and Charlie feed into a time-to-digital converter (TDC), which connects to a computer with a database. We have created a graphical user interface (GUI) that enables live data visualization of photons statistics, flexibility in defining coincidence windows and acquisition times for measuring single detector rates, twofold and threefold coincidences across multiple detectors (Figure 1.4).

In addition, we have created GUIs and python scripts to remotely monitor and control experimental variables such as the temperature and voltage setpoint of the MZI (which uses a thermoelectric crystal to control its phase A), the bias voltage inputs of the IMs, and the output power of the IMs. By frequently

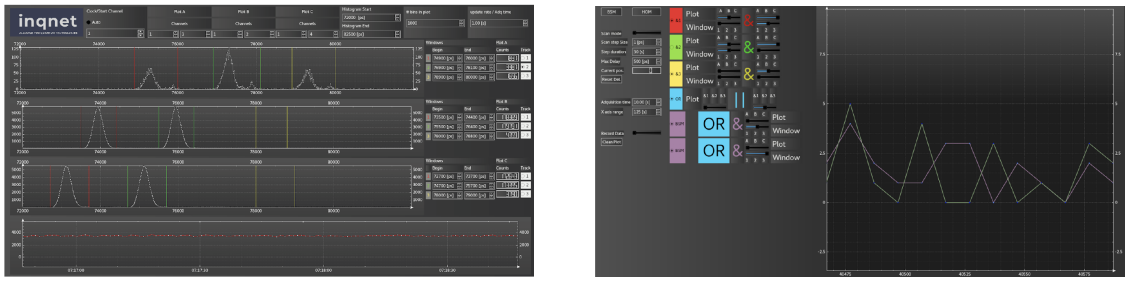

(a) Histograms of photon time-of-arrival with adjustable coincidence windows

(b) Settings and plots of coincidence logic, including the Bell state measurement

Figure 1.4: Graphical user interface for data visualization and storage

measuring and storing these experimental parameters, we are able to perform automated powervoltage IM feedbacks, interferometric phase scans, and data analysis that ensure long-term stability of our system and observation of real-time teleportation fidelities.

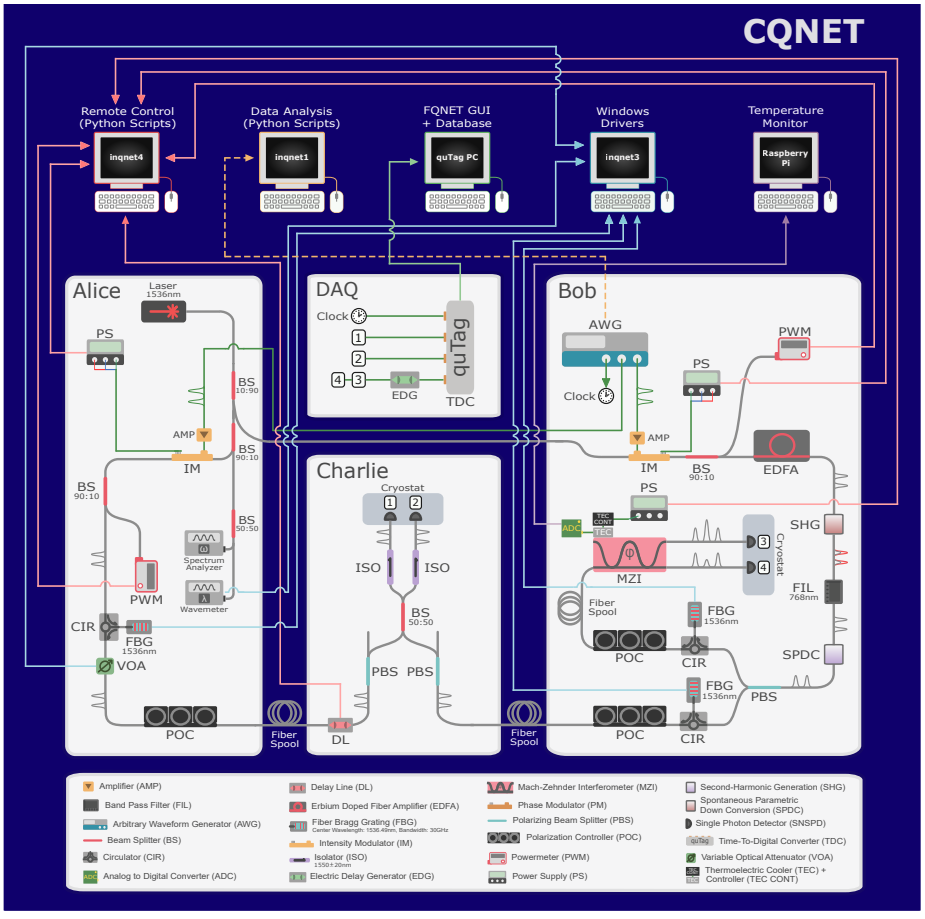

Figure 1.5: Blueprint of CQNET semi-automated systems integration for remote monitoring, optimization feedbacks and DAQ

1.2.3 Results

We characterized our system by measuring entanglement visibility, Hong-Ou- Mandel (HOM) visibility, and teleportation fidelity.

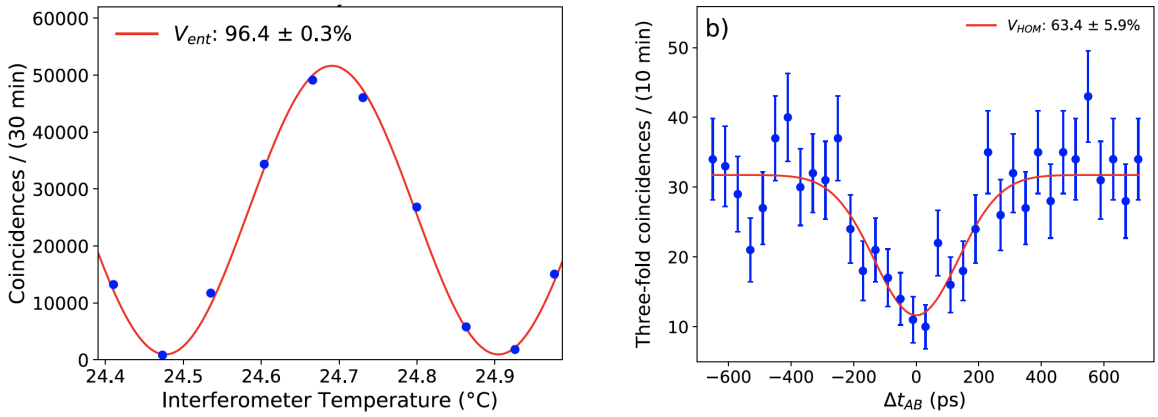

(a) Entanglement Visibility

(b) Hong-Ou-Mandel Dip

Figure 1.6: Characterization of entanglement visibility and indistinguishability for CQNET [16]

Entanglement Visibility

Entanglement visibility measures the quality of an entanglement source. To determine the entanglement visibility, we first connected the outputs of the PBS after SPDC to the inputs of the MZI. In this configuration, we were able to observe the correlations of the entangled photons as a function of the interferometric phase A by sweeping over the temperature and measuring coincidences at the two outputs of the MZI. We determined an entanglement visibility (V_{ent}) of $96.4 \pm 0.3\%$ using a fit to the data (Figure 1.6).

HOM Visibility

Next, we measured the HOM visibility to quantify the indistinguishability of the photons that interfere at Charlies beamsplitter. For a beamsplitter with a single photon incident at each input, the HOM effect predicts zero coincidences between the two outputs: the photons destructively interfere such that both photons appear at either one output or the other. We measured the HOM dip by delaying the timing of photons at one input with respect to the other and observing the drop in coincidences of Charlies beamsplitter outputs (conditioned on a detection at Bob) when the photons overlapped. We determined a HOM visibility (V_{HOM}) of $63.3 \pm 5.9\%$ using a fit to the data (Figure 1.6).

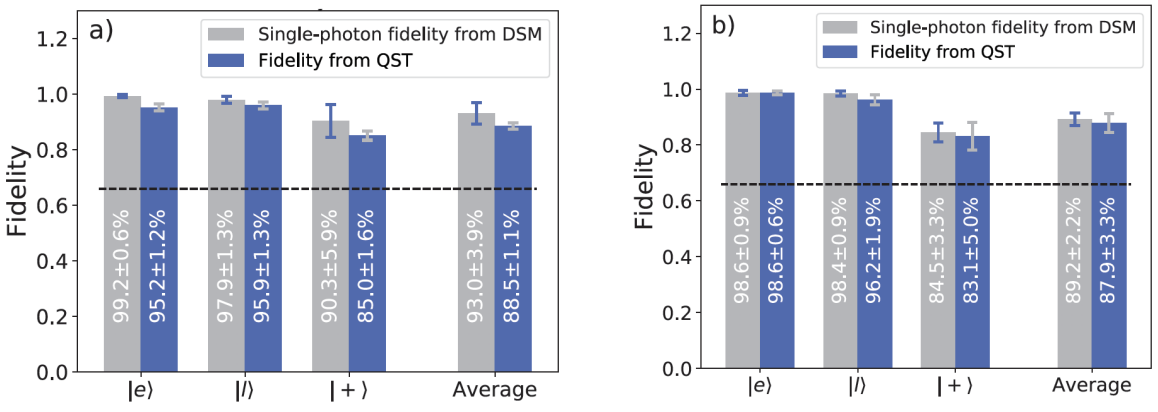

(a) Without spools

(b) With spools (45km total)

Figure 1.7: Teleportation fidelities a) without and b) with the 45 km total fiber spools depicted in the setup (Figure 1.3) [16]

Teleportation Fidelity

The most important metric is the teleportation fidelity, which corresponds to the probability that a qubit is successfully teleported. An arbitrary qubit can be constructed from a linear combination of

the X basis ($|+\rangle = |e\rangle + |l\rangle$, $|-\rangle = |e\rangle - |l\rangle$) Y basis ($|L\rangle = |e\rangle + i\,|l\rangle$, $|R\rangle = |e\rangle - i\,|l\rangle$), and Z basis ($|e\rangle, |l\rangle$) states. The overall teleportation fidelity is the average of the fidelities in each basis. We report average teleportation fidelities calculated from two approaches: quantum state tomography (QST) and decoy state method (DSM). We first calculated the fidelities of $|e\rangle$, $|l\rangle$, $|+\rangle$ by dividing the number of successful teleportation events by the total number of trials for each state. In the QST approach, we used these empirical fidelities to fit the nearest physical density matrices of the teleported qubits, and in turn calculated the fidelities from the best-fit density matrices. We report an average fidelity of $88.5 \pm 1.1\%$ without ($87.9 \pm 3.3\%$ with) the the fiber spools (Figure 1.7). In the DSM approach, we performed a decoy state analysis to extract multiphoton noise from our data and estimate the true single photon fidelities. We report an average fidelity of $93.0 \pm 3.9\%$ without ($89.2 \pm 2.2\%$ with) fiber spools using DSM (Figure 1.7).

1.2.4 Summary

Our teleportation system achieves average teleportation fidelities of $\sim 90\%$, the current record for long-distance optical fiber networks, using off-the-shelf components that are compatible with near term quantum hardware. Remote software, graphical interfaces and data storage ensure long term stability of $\geq 95\%$ Z basis teleportation fidelity over a week.

Improvements in progress include increasing teleportation rates and distances, reducing multiphoton noise, and free running field demonstrations of the teleportation systems with physically separate nodes of Alices, Bobs and Charlies. Our system serves as the basis for a quantum network with nodes at Caltech and Fermilab, a step towards DOEs proposed quantum internet backbone that will connect the 17 DOE National Labs.

1.3 Theory of Experimental Realization of Quantum Teleportation with Time-bin Qubits

1.3.1 Creating Time-bin Qubits with an Intensity Modulator

1.3.2 Bell State Measurement with a Beam Splitter

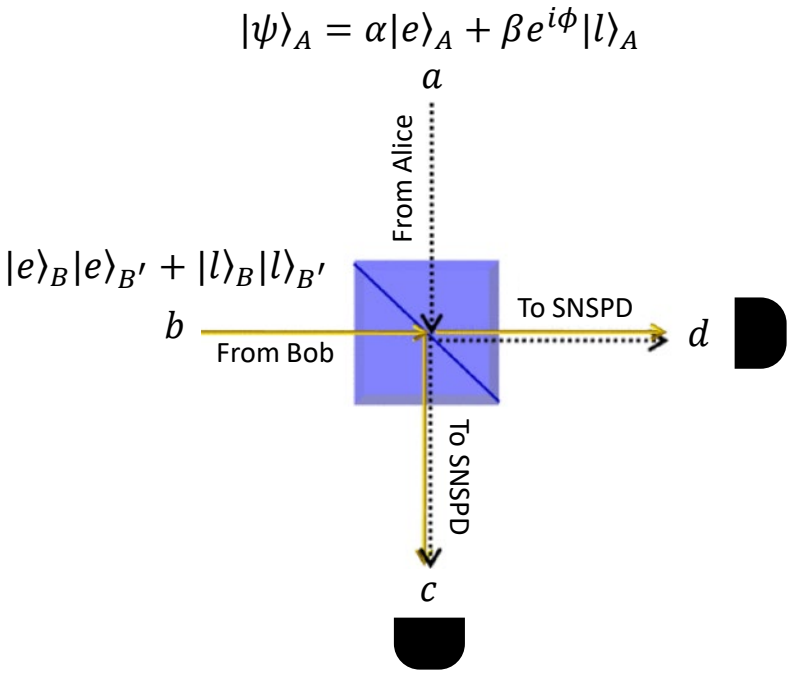

Figure 1.8: **Bell State Measurement**

Let $|\psi\rangle_a$, $|\psi\rangle_b$ represent modes at inputs a and b of the beamsplitter. By inputting Alice's photon (photon A) at input a and one of Bob's entangled photons (photon B) at input b, the input state of the beamsplitter $|\psi\rangle_{in}$ is:

$$|\psi\rangle_{in} = \frac{1}{\sqrt{2}}(\alpha\,|e\rangle_a + \beta e^{i\phi}\,|\ell\rangle_a) \otimes (|e\rangle_b\,|e\rangle_{B'} + |\ell\rangle_b\,|\ell\rangle_{B'}) \tag{1.17}$$

Let $|\psi\rangle_c$, $|\psi\rangle_d$ represent modes at outputs c and d. The beamsplitter transformations for $|\psi\rangle_a$ and $|\psi\rangle_b$ are

$$|\psi\rangle_a \to \frac{1}{\sqrt{2}}(|\psi\rangle_c + i\,|\psi\rangle_d) \tag{1.18}$$

$$|\psi\rangle_b \to \frac{1}{\sqrt{2}}(i\,|\psi\rangle_c + |\psi\rangle_d) \tag{1.19}$$

Transforming the input state in (1.17) according to (1.18) and (1.19), we find

$$\begin{aligned} |\psi\rangle_{out} &= \frac{1}{2\sqrt{2}}(\alpha(|e\rangle_c + i\,|e\rangle_d) + \beta e^{i\phi}(|\ell\rangle_c + i\,|\ell\rangle_d)) \otimes ((i\,|e\rangle_c + |e\rangle_d)\,|e\rangle_{B'} + (i\,|\ell\rangle_c + |\ell\rangle_d)\,|\ell\rangle_{B'}) \\ &= \frac{1}{2\sqrt{2}}(\alpha\,|e\rangle_c + \alpha i\,|e\rangle_d + \beta e^{i\phi}\,|\ell\rangle_c + i\beta e^{i\phi}\,|\ell\rangle_d) \otimes (i\,|e\rangle_c\,|e\rangle_{B'} + |e\rangle_d\,|e\rangle_{B'} + i\,|\ell\rangle_c\,|\ell\rangle_{B'} + |\ell\rangle_d\,|\ell\rangle_{B'}) \end{aligned} \tag{1.20}$$

Consider terms corresponding to coincidences at c and d:

$$|\psi\rangle_{out} = \frac{1}{2\sqrt{2}}(\alpha\,|e\rangle_c\,|\ell\rangle_d\,|\ell\rangle_{B'} - \alpha\,|\ell\rangle_c\,|e\rangle_d\,|\ell\rangle_{B'} + \beta e^{i\phi}\,|\ell\rangle_c\,|e\rangle_d\,|e\rangle_{B'} - \beta e^{i\phi}\,|e\rangle_c\,|\ell\rangle_d\,|e\rangle_{B'} + ...) \tag{1.21}$$

By rearranging $|\psi\rangle_{out}$, we find

$$\begin{aligned} |\psi\rangle_{out} &= \frac{1}{4}\big((|e\rangle_c\,|\ell\rangle_d - |\ell\rangle_c\,|e\rangle_d)(\alpha\,|\ell\rangle_{B'} - \beta e^{i\phi}\,|e\rangle_{B'}) + ...\big) \\ &= \frac{1}{4}\big(\,|\Psi^-\rangle_{cd}\,(\alpha\,|\ell\rangle_{B'} - \beta e^{i\phi}\,|e\rangle_{B'}) + ...\big) \end{aligned} \tag{1.22}$$

Note that this is the same as the $|\Psi^-\rangle$ term in the output of the teleportation protocol. Experimentally, we perform the Bell State measurement of $|\Psi^-\rangle$ by measuring the coincidences between $|e\rangle$ at c, $|\ell\rangle$ at d and $|\ell\rangle$ at c, $|e\rangle$ at d using the FQNET GUI.

1.3.3 Projective Measurement with an Interferometer

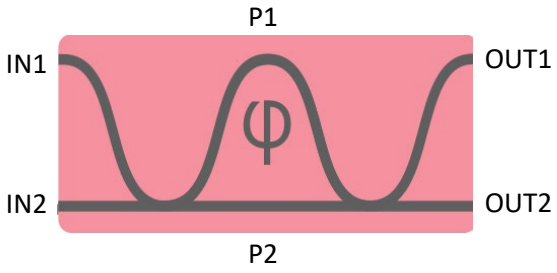

Figure 1.9: **Mach-Zehnder Interferometer**

In our set-up, Bob uses an interferometer to measure the state of his qubit and verify teleportation. Bob inputs his photon into the interferometer and tunes the phase φ of the interferometer to make a projective measurement onto a desired state. Consider an input mode of $|\psi\rangle_{\text{IN1}} = \gamma\,|e\rangle_{\text{IN1}} + \delta e^{i\theta}\,|\ell\rangle_{\text{IN1}}$ at IN1 and vacuum at IN2. Since $|\psi\rangle_{\text{IN1}} \to i\,|\psi\rangle_{\text{P1}} + |\psi\rangle_{\text{P2}}$, the mode at IN1 transforms to modes at path 1 (P1) and path 2 (P2) as:

$$|\psi\rangle_{\text{IN1}} = \gamma\,|e\rangle_{\text{IN1}} + \delta e^{i\theta}\,|\ell\rangle_{\text{IN1}} \to \gamma(i\,|e\rangle_{\text{P1}} + |e\rangle_{\text{P2}}) + \delta e^{i\theta}(i\,|\ell\rangle_{\text{P1}} + |\ell\rangle_{\text{P2}}) \tag{1.23}$$

P1 introduces an additional time delay and variable phase φ difference with respect to P2. The path length of P1 is chosen such that photons that travel through P1 transform as:

$$\begin{aligned} |e\rangle &\to e^{i\varphi} |\ell\rangle \\ |\ell\rangle &\to e^{i\varphi} |\ell'\rangle \end{aligned} \tag{1.24}$$

where the time delay between $|\ell'\rangle$ and $|\ell\rangle$ = time delay between $|\ell\rangle$ and $|e\rangle$. Thus, between the inputs and outputs of the interferometer, the state of the photon transforms to:

$$\gamma(i\,|e\rangle_{\mathrm{P1}} + |e\rangle_{\mathrm{P2}}) + \delta e^{i\theta}(i\,|\ell\rangle_{\mathrm{P1}} + |\ell\rangle_{\mathrm{P2}}) \to \gamma(ie^{i\varphi}\,|\ell\rangle_{\mathrm{P1}} + |e\rangle_{\mathrm{P2}}) + \delta e^{i\theta}(ie^{i\varphi}\,|\ell'\rangle_{\mathrm{P1}} + |\ell\rangle_{\mathrm{P2}}) \tag{1.25}$$

Finally, Since $|\psi\rangle_{\mathrm{P1}} \to i\,|\psi\rangle_{\mathrm{OUT1}} + |\psi\rangle_{\mathrm{OUT2}}$ and $|\psi\rangle_{\mathrm{P2}} \to |\psi\rangle_{\mathrm{OUT1}} + i\,|\psi\rangle_{\mathrm{OUT2}}$, the P1 and P2 modes transform to OUT1 and OUT2 modes as:

$$\begin{aligned} \gamma(ie^{i\varphi}\,|\ell\rangle_{\mathrm{P1}} + |e\rangle_{\mathrm{P2}}) + \delta e^{i\theta}(ie^{i\varphi}\,|\ell'\rangle_{\mathrm{P1}} + |\ell\rangle_{\mathrm{P2}}) \to \gamma(ie^{i\varphi}(i\,|\ell\rangle_{\mathrm{OUT1}} + |\ell\rangle_{\mathrm{OUT2}}) + \\ (|e\rangle_{\mathrm{OUT1}} + i\,|e\rangle_{\mathrm{OUT2}})) + \delta e^{i\theta}(ie^{i\varphi}(i\,|\ell'\rangle_{\mathrm{OUT1}} + |\ell'\rangle_{\mathrm{OUT2}}) + (|\ell\rangle_{\mathrm{OUT1}} + i\,|\ell\rangle_{\mathrm{OUT2}})) \end{aligned} \tag{1.26}$$

Thus the overall transformation of the interferometer on $|\psi\rangle_{\mathrm{IN1}}$ is:

$$\begin{aligned} \gamma\,|e\rangle_{\mathrm{IN1}} + \delta e^{i\theta}\,|\ell\rangle_{\mathrm{IN1}} \to \gamma\,|e\rangle_{\mathrm{OUT1}} + e^{i(\varphi+\pi)}(\gamma + \delta e^{i(\theta-\varphi-\pi)})\,|\ell\rangle_{\mathrm{OUT1}} + \delta e^{i(\theta+\varphi+\pi)}\,|\ell'\rangle_{\mathrm{OUT1}} \\ i\gamma\,|e\rangle_{\mathrm{OUT2}} + ie^{i\varphi}(\gamma + \delta e^{i(\theta-\varphi)})\,|\ell\rangle_{\mathrm{OUT2}} + i\delta e^{i(\theta+\varphi)}\,|\ell'\rangle_{\mathrm{OUT2}} \end{aligned} \tag{1.27}$$

Consider the case where $\varphi = \theta$. Then the output state $|\psi\rangle_{\mathrm{OUT}}$ is

$$\begin{aligned} |\psi\rangle^{\mathrm{OUT}} = \gamma\,|e\rangle^{\mathrm{OUT1}} + e^{i(\theta+\pi)}(\gamma - \delta)\,|\ell\rangle^{\mathrm{OUT1}} + \delta e^{i(2\theta+\pi)}\,|\ell'\rangle^{\mathrm{OUT1}} \\ i\gamma\,|e\rangle^{\mathrm{OUT2}} + ie^{i\theta}(\gamma + \delta)\,|\ell\rangle^{\mathrm{OUT2}} + i\delta e^{i(2\theta)}\,|\ell'\rangle^{\mathrm{OUT2}} \end{aligned} \tag{1.28}$$

When $\varphi = \theta + \pi$, then

$$\begin{aligned} |\psi\rangle_{\mathrm{OUT}} = \gamma\,|e\rangle_{\mathrm{OUT1}} + e^{i\theta}(\gamma + \delta)\,|\ell\rangle_{\mathrm{OUT1}} + \delta e^{i(2\theta)}\,|\ell'\rangle_{\mathrm{OUT1}} \\ i\gamma\,|e\rangle_{\mathrm{OUT2}} + ie^{i(\theta+\pi)}(\gamma - \delta)\,|\ell\rangle_{\mathrm{OUT2}} + i\delta e^{i(2\theta+\pi)}\,|\ell'\rangle_{\mathrm{OUT2}} \end{aligned} \tag{1.29}$$

We use this interference effect to verify the state of Bob's qubit and see if teleportation was successful.

FQNET GUI Logic

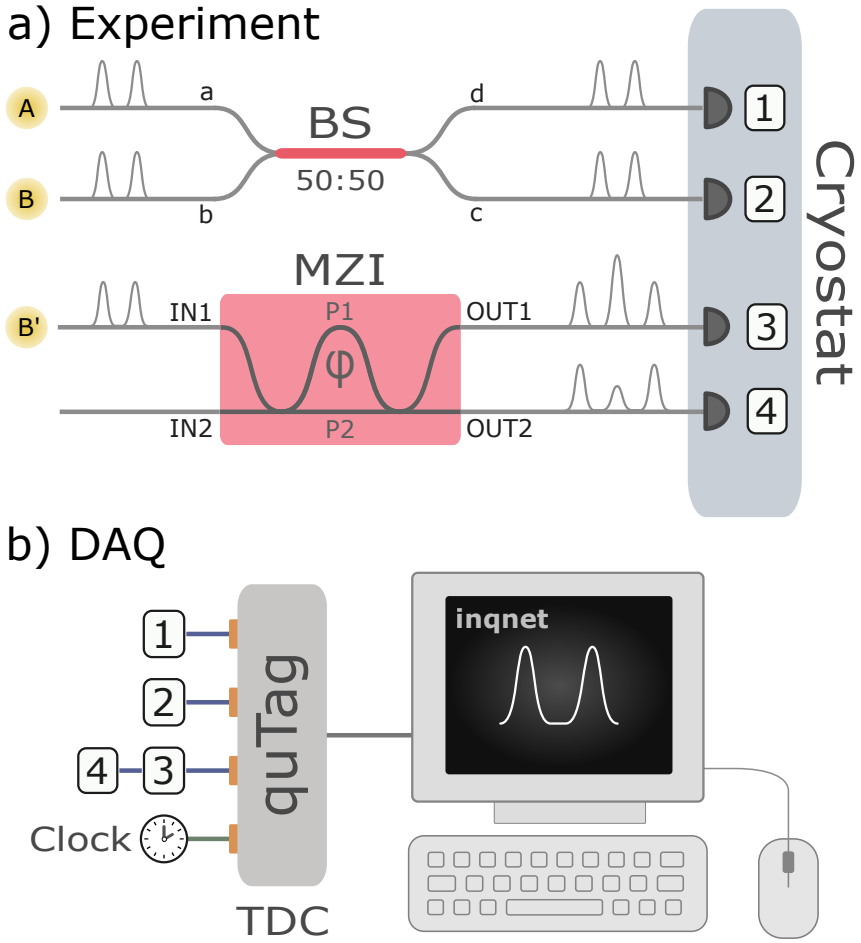

Figure 1.10: **CQNET Teleportation Measurement**

Chapter 2

SPDC Characterization with Binary Threshold and PNR SNSPDs

2.1 PDC State Generation

$$\hat{H}_{PDC} \propto \chi^{(2)} \int d^3r \hat{E}_p^{(-)}(\vec{r},t)\hat{E}_s^{(+)}(\vec{r},t)\hat{E}_i^{(+)}(\vec{r},t) + H.c. \tag{2.1}$$

$$|\psi\rangle_{PDC} = \exp\left\{-\frac{i}{\hbar}\left(B\sum_{k,l}\int\int d\omega_s d\omega_i f_{k,l}(\omega_s,\omega_i) \times \hat{a}_k^{(s)\dagger}(\omega_s)\hat{a}_l^{(i)\dagger(\omega_i)} + H.c.\right)\right\}|0\rangle \tag{2.2}$$

2.2 Generation of single photons from SPDC

$$\hat{H}_I = \hbar\lambda\hat{a}_s^\dagger\hat{a}_i^\dagger + H.c. \tag{2.3}$$

$$|\psi\rangle_{SPDC} = e^{-it\hat{H}_I/\hbar}|\Psi(0)\rangle \approx \sum_{n=0}^{\infty}\frac{(-it\lambda\hat{a}_s^\dagger\hat{a}_i^\dagger)^n}{n!}|0_s,0_i\rangle = \sum_{n=0}^{\infty}\frac{(-i\mu)^n}{n!}|n_s,n_i\rangle \tag{2.4}$$

where $\lambda \propto \chi^{(2)}\epsilon_p$, $\mu = \lambda t$.

2.3 Generation of quadrature squeezed light

$$\hat{H} = \hbar\omega\hat{a}^\dagger\hat{a} + \hbar\omega_p\hat{b}^\dagger\hat{b} + i\hbar\chi^{(2)}(\hat{a}^2\hat{b}^\dagger - \hat{a}^{\dagger 2}\hat{b}) \tag{2.5}$$

Take $\hat{b} \to \beta e^{-i\omega_p t}$, $\hat{b}^\dagger \to \beta^* e^{i\omega_p t}$, since pumping with strong coherent light, so pump state $\left|\beta e^{-i\omega_p t}\right\rangle$ is eigenstate of $\hat{b}$. Dropping irrelevant terms and using parametric approximation,

$$\hat{H}^{(PA)} = \hbar\omega\hat{a}^\dagger\hat{a} + i\hbar(\gamma^*\hat{a}^2e^{i\omega_p t} - \gamma\hat{a}^{\dagger 2}e^{-i\omega_p t}) \tag{2.6}$$

where $\gamma = \chi^{(2)}\beta$.

$$\hat{H}_I(t) = i\hbar(\gamma^*\hat{a}^2e^{i(\omega_p-2\omega)t} - \gamma\hat{a}^{\dagger 2}e^{-i(\omega_p-2\omega)t}) \tag{2.7}$$

For $\omega_p = 2\omega$, $\hat{H}_I = i\hbar(\gamma^*\hat{a}^2 - \gamma\hat{a}^{\dagger 2})$.

The corresponding time evolution operator takes the form of the squeeze operator:

$$|\psi\rangle_{DPDC} = e^{-i\hat{H}_I t/\hbar}|0\rangle = e^{\gamma^* t\hat{a}^2 - \gamma t\hat{a}^{\dagger 2}}|0\rangle \tag{2.8}$$

Identifying the output photons as "idler" and "signal" photons, using $\hat{A}$ for the signal beam and $\hat{B}$ for the idler beam, and taking γt, $\gamma^* t \to r$, and setting phase factor to π, we get:

$$|\psi\rangle_{DPDC} = e^{r\hat{A}^\dagger\hat{B}^\dagger - r\hat{A}\hat{B}}|0_s,0_i\rangle = \mathrm{sech}(r)\sum_{n=0}^{\infty}\tanh^n(r)|n_s,n_i\rangle \tag{2.9}$$

2.4 Heralding Single Photons from Single-Mode PDC Sources

Given detector efficiency η, the positive operator valued measure (POVM) for binary detection are:

$$\hat{\Pi}_{\text{“No Click”}} = \sum_{n=0}^{\infty}(1-\eta)^n \left|n\right\rangle \left\langle n\right| \tag{2.10}$$

$$\hat{\Pi}_{\text{“Click”}} = \sum_{n=0}^{\infty}[1-(1-\eta)^n] \left|n\right\rangle \left\langle n\right| \tag{2.11}$$

The POVM elements of a general photon-number resolving detector measuring n photons are given by:

$$\hat{\Pi}(n) = \sum_{N=n}^{\infty}\binom{N}{n}(1-\eta)^{N-n}\eta^n \left|N\right\rangle \left\langle N\right| \tag{2.12}$$

For the detection of a single photon (the case that we are interested in), we set $n = 1$ in the expression above:

$$\hat{\Pi}(1) = \sum_{N=1}^{\infty}\binom{N}{1}(1-\eta)^{N-1}\eta \left|N\right\rangle \left\langle N\right| = \sum_{N=1}^{\infty} N(1-\eta)^{N-1}\eta \left|N\right\rangle \left\langle N\right| \tag{2.13}$$

The POVMs have the same structure and are of form:

$$\hat{\Pi}_{c_n} = \sum_{n=0}^{\infty} c_n \left|n\right\rangle \left\langle n\right| \tag{2.14}$$

In the binary case,

$$c_n = 1-(1-\eta)^n \tag{2.15}$$

whereas in the PNR case,

$$c_n = \sum_{N=n}^{\infty}\binom{N}{n}(1-\eta)^{N-n}\eta^n \tag{2.16}$$

The probability of a successful heralding event is:

$$p_s(r, c_n) = \left\langle \psi\right|_{PDC} \hat{\Pi}_{c_n} \left|\psi\right\rangle_{PDC} \tag{2.17}$$

The heralded signal state after a successful detection takes the form:

$$\rho_s(r, c_n) = \frac{tr_i(\hat{\Pi}_{c_n} \left|\psi\right\rangle_{PDC PDC} \left\langle \psi\right|)}{{}_{PDC}\left\langle \psi\right| \hat{\Pi}_{c_n} \left|\psi\right\rangle_{PDC}} \tag{2.18}$$

The fidelity of the heralded signal state after a successful detection of a pure single photon is:

$$F(r, c_n) = \left\langle 1_s\right| \rho_s \left|1_s\right\rangle \tag{2.19}$$

Note that $c_1 = \eta$ for the binary case and the PNR case in this formalism.

2.4.1 Finding p_s, ρ_s, and F for $\left|\psi\right\rangle_{SPDC}$

The probability of a successful heralding event is:

$$p_s(r, c_n) = {}_{SPDC}\left\langle \psi\right| \hat{\Pi}_{c_n} \left|\psi\right\rangle_{SPDC} \tag{2.20}$$

$$p_s(\mu, c_n) = \sum_{\ell=0}^{\infty}\sum_{m=0}^{\infty}\sum_{n=0}^{\infty} \frac{(i\mu)^\ell}{\ell!} \left\langle \ell_s, \ell_i\right| c_m \left|m_s, m_i\right\rangle \left\langle m_s, m_i\right| \frac{(-i\mu)^n}{n!} \left|n_s, n_i\right\rangle \tag{2.21}$$

$$p_s(\mu, c_n) = \sum_{n=0}^{\infty}\left(\frac{\mu^n}{n!}\right)^2 c_n \tag{2.22}$$

To find the heralded signal state after successful detection:

$$tr_i(\hat{\Pi}_{c_n} |\psi\rangle_{SPDCSPDC} \langle\psi|) = \sum_{k=0}^{\infty}\sum_{\ell=0}^{\infty}\sum_{m=0}^{\infty}\sum_{n=0}^{\infty} \langle k_i| c_\ell |\ell_s, \ell_i\rangle \langle \ell_s, \ell_i| \frac{(-i\mu)^m}{m!}\frac{(i\mu)^n}{n!} |m_s, m_i\rangle \langle n_s, n_i|k_i\rangle \tag{2.23}$$

$$tr_i(\hat{\Pi}_{c_n} |\psi\rangle_{SPDCSPDC} \langle\psi|) = \sum_{n=0}^{\infty} c_n \left(\frac{\mu^n}{n!}\right)^2 |n_s\rangle \langle n_s| \tag{2.24}$$

So, the heralded signal state is:

$$\rho_s(\mu, c_n) = \frac{\sum_{n=0}^{\infty} c_n \left(\frac{\mu^n}{n!}\right)^2 |n_s\rangle \langle n_s|}{\sum_{n=0}^{\infty}\left(\frac{\mu^n}{n!}\right)^2 c_n} \tag{2.25}$$

The fidelity is:

$$F(\mu, c_n) = \frac{\sum_{n=0}^{\infty} c_n \left(\frac{\mu^n}{n!}\right)^2 \langle 1_s|n_s\rangle \langle n_s|1_s\rangle}{\sum_{n=0}^{\infty}\left(\frac{\mu^n}{n!}\right)^2 c_n} \tag{2.26}$$

$$F(\mu, c_n) = \frac{c_1\mu^2}{\sum_{n=0}^{\infty}\left(\frac{\mu^n}{n!}\right)^2 c_n} \tag{2.27}$$

Therefore, $p_s(\mu, c_n)F(\mu, c_n) = c_1\mu^2$.

Binary Detector

Since $c_1 = \eta$ for a binary detector, for SPDC production we find:

$$p_s(\mu, c_n) = \sum_{n=0}^{\infty}\left(\frac{\mu^n}{n!}\right)^2 [1 - (1-\eta)^n] \tag{2.28}$$

$$F(\mu, c_n) = \frac{\eta\mu^2}{\sum_{n=0}^{\infty}\left(\frac{\mu^n}{n!}\right)^2 [1 - (1-\eta)^n]} \tag{2.29}$$

PNR Detector

Since $c_1 = \sum_{N=1}^{\infty} N(1-\eta)^{N-1}\eta$ for a PNR detector, for SPDC production we find:

$$p_s(\mu, c_n) = \sum_{n=0}^{\infty}\left(\frac{\mu^n}{n!}\right)^2 [\sum_{N=n}^{\infty}\binom{N}{n}(1-\eta)^{N-n}\eta^n] \tag{2.30}$$

$$F(\mu, c_n) = \frac{(1/\eta)\mu^2}{\sum_{n=0}^{\infty}\left(\frac{\mu^n}{n!}\right)^2 [\sum_{N=n}^{\infty}\binom{N}{n}(1-\eta)^{N-n}\eta^n]} \tag{2.31}$$

However, there exists a $p_{th}^{(max)} = \nu = 0.25$. This comes from the thermal photon distribution $P_n = \frac{\bar{n}^n}{(1+\bar{n})^{n+1}}$, which equals 0.25 for $\bar{n} = n = 1$. As such, we have to scale p_s by ν:

$$p_s(\mu, c_n) = \nu\sum_{n=0}^{\infty}\left(\frac{\mu^n}{n!}\right)^2 [\sum_{N=n}^{\infty}\binom{N}{n}(1-\eta)^{N-n}\eta^n] \tag{2.32}$$

2.4.2 Finding p_s, ρ_s, and F for $|\psi\rangle_{DPDC}$

The probability of a successful heralding event is:

$$p_s(r,c_n) = {}_{DPDC}\langle\psi|\,\hat{\Pi}_{c_n}\,|\psi\rangle_{DPDC} \tag{2.33}$$

$$p_s(r,c_n) = \mathrm{sech}^2(r)\sum_{\ell=0}^{\infty}\sum_{m=0}^{\infty}\sum_{n=0}^{\infty}\tanh^{\ell}(r)\,\langle\ell_s,\ell_i|\,c_m\,|m_s,m_i\rangle\,\langle m_s,m_i|\tanh^{n}(r)\,|n_s,n_i\rangle \tag{2.34}$$

$$p_s(r,c_n) = \mathrm{sech}^2(r)\sum_{n=0}^{\infty}c_n\tanh^{2n}(r) \tag{2.35}$$

To find the heralded signal state after successful detection:

$$tr_i(\hat{\Pi}_{c_n}\,|\psi\rangle_{DPDCDPDC}\,\langle\psi|) = \mathrm{sech}^2(r)\sum_{k=0}^{\infty}\sum_{\ell=0}^{\infty}\sum_{m=0}^{\infty}\sum_{n=0}^{\infty}\langle k_i|\,c_\ell\,|\ell_s,\ell_i\rangle\,\langle\ell_s,\ell_i|\tanh^{m}(r)\tanh^{n}(r)\,|m_s,m_i\rangle\,\langle n_s,n_i|k_i\rangle \tag{2.36}$$

$$tr_i(\hat{\Pi}_{c_n}\,|\psi\rangle_{SPDCSPDC}\,\langle\psi|) = \mathrm{sech}^2(r)\sum_{n=0}^{\infty}c_n\tanh^{2n}(r)\,|n_s\rangle\,\langle n_s| \tag{2.37}$$

So, the heralded signal state is:

$$\rho_s(\mu,c_n) = \frac{\sum_{n=0}^{\infty}c_n\tanh^{2n}(r)\,|n_s\rangle\,\langle n_s|}{\sum_{n=0}^{\infty}c_n\tanh^{2n}(r)} \tag{2.38}$$

The fidelity is:

$$F(\mu,c_n) = \frac{\sum_{n=0}^{\infty}c_n\tanh^{2n}(r)\,\langle 1_s|n_s\rangle\,\langle n_s|1_s\rangle}{\sum_{n=0}^{\infty}c_n\tanh^{2n}(r)} \tag{2.39}$$

$$F(\mu,c_n) = \frac{c_1\tanh^2(r)}{\sum_{n=0}^{\infty}c_n\tanh^{2n}(r)} \tag{2.40}$$

Therefore, $p_s(\mu,c_n)F(\mu,c_n) = c_1\mathrm{sech}^2(r)\tanh^2(r)$.

Binary Detector

Since $c_1 = \eta$ for a binary detector, for DPDC production we find:

$$p_s(r,c_n) = \mathrm{sech}^2(r)\sum_{n=0}^{\infty}[1-(1-\eta)^n]\tanh^{2n}(r) \tag{2.41}$$

$$F(\mu,c_n) = \frac{\eta\tanh^2(r)}{\sum_{n=0}^{\infty}[1-(1-\eta)^n]\tanh^{2n}(r)} \tag{2.42}$$

PNR Detector

Since $c_1 = \sum_{N=1}^{\infty}N(1-\eta)^{N-1}\eta$ for a PNR detector, for DPDC production we find:

$$p_s(r,c_n) = \mathrm{sech}^2(r)\sum_{n=0}^{\infty}[\sum_{N=n}^{\infty}\binom{N}{n}(1-\eta)^{N-n}\eta^n]\tanh^{2n}(r) \tag{2.43}$$

$$F(\mu,c_n) = \frac{(1/\eta)\tanh^2(r)}{\sum_{n=0}^{\infty}[\sum_{N=n}^{\infty}\binom{N}{n}(1-\eta)^{N-n}\eta^n]\tanh^{2n}(r)} \tag{2.44}$$

However, there exists a $p_{th}^{(max)} = \nu = 0.25$. This comes from the thermal photon distribution $P_n = \frac{\bar{n}^n}{(1+\bar{n})^{n+1}}$, which equals 0.25 for $\bar{n} = n = 1$. As such, we have to scale p_s by ν:

$$p_s(r,c_n) = \nu\mathrm{sech}^2(r)\sum_{n=0}^{\infty}[\sum_{N=n}^{\infty}\binom{N}{n}(1-\eta)^{N-n}\eta^n]\tanh^{2n}(r) \tag{2.45}$$

2.5 Heralding Single Photons with Switched (Multiplexed) PDC Sources

Given a photon heralding probability of ν, lossless routing, PNR detectors, and N_s sources the overall heralding probability for SPDC is:

$$p_s(\mu, c_n) = [1-(1-\nu)^{N_s}] \sum_{n=0}^{\infty} \left(\frac{\mu^n}{n!}\right)^2 [\sum_{N=n}^{\infty} \binom{N}{n} (1-\eta)^{N-n} \eta^n] \tag{2.46}$$

and for DPDC is:

$$p_s(\nu, \eta, r) = [1-(1-\nu)^{N_s}] \mathrm{sech}^2(r) \sum_{n=0}^{\infty} [\sum_{N=n}^{\infty} \binom{N}{n} (1-\eta)^{N-n} \eta^n] \tanh^{2n}(r) \tag{2.47}$$

Chapter 3

Modeling the $g^{(2)}(0)$ Experiment for Heralded Single Photon Source Enhancement using PNR SNSPDs

3.1 Introduction

Single photon pair sources essential for quantum communication, e.g. as entanglement sources and heralded single photon sources (HSPS). However, convenient production mechanisms like spontaneous parametric down conversion (SPDC) are probabilistic in nature, not deterministic. The single photon pair probability for SPDC caps at only 25%, so multiphoton pairs manifest as significant noise source at high mean photon number μ. Therefore, quantum communication experiments using SPDC have historically been limited to low μ, i.e. quantum communication rates.

One work-around is to have photon number resolving (PNR) detectors. If detectors can distinguish between 0, 1, and >1 photons, then we can filter out multiphoton noise by triggering the experiment only on the single photon pair events. This should enable experimental operation at higher μ.

For quantum communication experiments, superconducting nanowire single photon detectors (SNSPDs) are the preferred detectors due to their optimization across various metrics important to quantum communication, including low jitter and fast recovery time [7]. Historically, SNSPDs are threshold detectors, which can distinguish only between zero and nonzero numbers of photons. As such, quantum communication experiments typically need to run at very low μ to reduce mulitphoton events.

Through a collaboration with JPL, MIT, and NIST, there are SNSPDs now available that use differential readouts to realize intrinsic PNR capability in addition to low jitter, fast recovery time, and other important metrics. Our goal is to do the first demonstration of an experimental improvement using these PNR SNSPDs. In particular, we aim to show an enhancement in the quality of a heralded single photon source using SPDC.

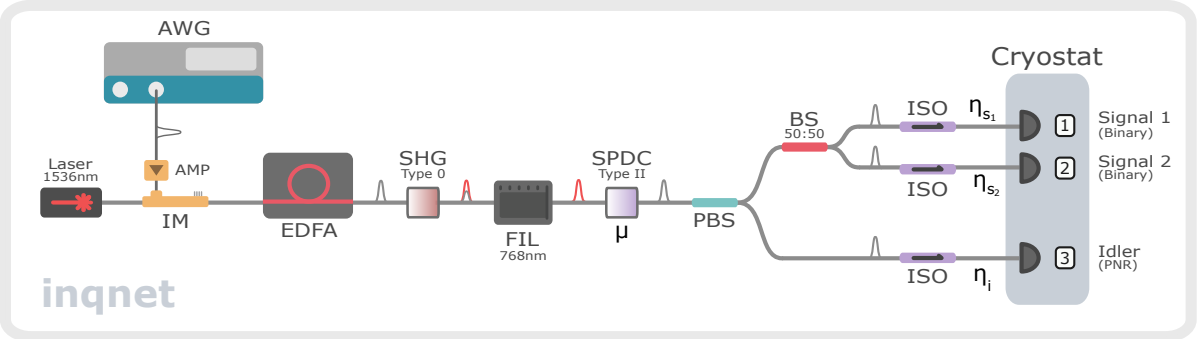

Figure 3.1: **Set-up of the HSPS $g^{(2)}(0)$ Experiment**

One way to measure the quality of an HSPS is to measure the second order correlation function

$g^{(2)}(0)$ defined as

$$g^{(2)}(0) = \frac{P(i, s_1, s_2)}{P(i, s_1)P(i, s_2)} \tag{3.1}$$

where $P(i, s_1, s_2)$ is the probability of threefold coincidence across the idler and two signal detectors, $P(i, s_1)$ is the probability of a twofold coincidence across the idler and signal 1 detector, and $P(i, s_1)$ is the probability of a twofold coincidence across the idler and signal 2 detector (e.g. per clock cycle). For a perfect single photon pair source, $g^{(2)}(0) = 0$, since only single pairs of photons are produced and the photon on the signal arm arrives to either the signal 1 or the signal 2 detector (never both). If we perform the experiment twice, (1) using only threshold detectors and (2) using a PNR detector for the idler and threshold detectors for signal 1 and 2, we expect that the $g^{(2)}(0)$ we measure in experiment (2) is less than the $g^{(2)}(0)$ in experiment (1), because in experiment (2) we trigger only on single photons events at the idler[1]. In this way, we aim to quantitatively show a statistically significant improvement in SPDC HSPS as a step towards significantly increased quantum communication rates using PNR SNSPDs.

3.2 Discrete Model of $g^{(2)}(0)$ Experiment

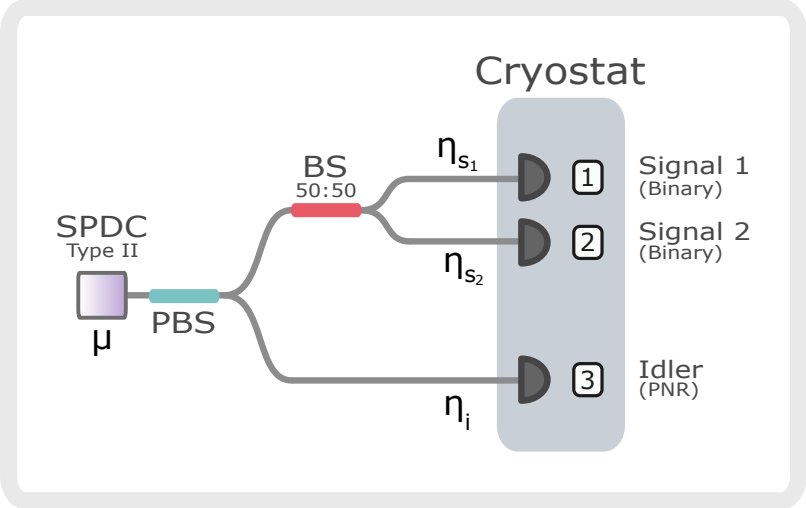

Figure 3.2: **Model Diagram**. This is the reduced diagram of the full experimental set up shown in Figure 3.1.

We model the setup depicted in Figure 3.1 as a source with mean photon number μ followed by a PBS with unity efficiency and a BS with unity efficiency on the signal arm (Figure 3.2). We define η_i, η_{s_1}, and η_{s_2} as the net efficiencies (including systemic losses and detector efficiency) observed by the idler, signal 1, and signal 2 detectors, respectively.

First, the probability of having n multiphoton pairs at the output of the SPDC is

$$P_n = \frac{(\tanh \zeta)^{2n}}{(\cosh \zeta)^2} \tag{3.2}$$

where μ is the mean photon number and ζ is the squeezing parameter (related to the pump power) and $\mu = (\sinh \zeta)^2$. In terms of μ, the probability of n photon pairs is:

$$P_n = \frac{\mu^n}{(1+\mu)^{n+1}} \tag{3.3}$$

At the signal arm, for n pairs of photons produced by the SPDC, we model the beamsplitter with a Fock state $|n\rangle$ mode at one input (a) and a vacuum state mode at the other input (b), according to

[1]For a perfect PNR idler detector, we expect $g^{(2)}(0) = 0$, but due to noise and non-unity discrimination and detection efficiencies, we expect $0 < g_2^{(2)}(0) < g_1^{(2)}(0)$, where $g_1^{(2)}(0)$ is the $g^{(2)}(0)$ for experiment (1) and $g_2^{(2)}(0)$ is the $g^{(2)}(0)$ for experiment (2)

Figure 3.3. The n incident photons at input mode a are binomially distributed at output modes c and d. This can be seen by applying the beamsplitter transformation to n incident photons at a, where $a^\dagger$, $b^\dagger$, $c^\dagger$, and $d^\dagger$ are the creation operators for modes a, b, c, and d, respectively.

$$(a^\dagger)^n \left|0_a\right\rangle \left|0_b\right\rangle \left|0_c\right\rangle \left|0_d\right\rangle \rightarrow \frac{1}{\sqrt{2}}^n (c^\dagger + id^\dagger)^n \left|0_a\right\rangle \left|0_b\right\rangle \left|0_c\right\rangle \left|0_d\right\rangle \tag{3.4}$$

The corresponding output wavefunction is[2]

$$\begin{aligned} \left|\psi_{cd}\right\rangle &= \frac{1}{\sqrt{2}}^n (c^\dagger + id^\dagger)^n \left|0_c\right\rangle \left|0_d\right\rangle \\ &\simeq \frac{1}{\sqrt{2}}^n \sum_{k=0}^{n} \binom{n}{k} (c^\dagger)^k (id^\dagger)^{n-k} \left|0_c\right\rangle \left|0_d\right\rangle \\ &\simeq \frac{1}{\sqrt{2}}^n \sum_{k=0}^{n} \binom{n}{k} i^{n-k} \left|k\right\rangle \left|n-k\right\rangle \end{aligned} \tag{3.5}$$

It can be shown that for n photon pairs incident to the beam splitter, the probability of measuring k photons at output c (signal detector 1) and $n-k$ photons at output d (signal detector 2) is

$$P_{c,d}(k, n-k) = \frac{\binom{n}{k}}{\sum_{k=0}^{n} \binom{n}{k}} = \frac{\binom{n}{k}}{2^n} \tag{3.6}$$

3.2.1 Dark Counts

Given the average dark counts per coincidence window per clock cycle (D), we can estimate the probability $P(n_d \geq 1)$ of getting at least one dark count n_d per coincidence window per clock cycle by dividing D by the clock rate. Since $P(n_d \geq 1)$ depends on the detector, we estimate $P(n_d \geq 1)$ separately for each detector by finding the dark counts in a 1 ns window per second and dividing by the rate. In terms of the probability $P(n_d = 1)$ of getting a single dark count per coincidence window per clock cycle, $P(n_d \geq 1)$ can be expressed as

$$P(n_d \geq 1) = \sum_{k=1}^{\infty} (P(n_d = 1))^k = \frac{P(n_d = 1)}{1 - P(n_d = 1)}. \tag{3.7}$$

In words, the probability of a binary detector registering a dark count is the probability of at least one "dark" photon[3] incident on the detector.

On the other hand, a PNR detector has the ability to resolve single photons, so the probability of the PNR detector "registering" the dark count[4] is $P(n_d = 1)$, as opposed to $P(n_d \geq 1)$ in the binary case. In terms of $P(n_d \geq 1)$, which is what we measure experimentally, $P(n_d = 1)$ is simply

$$P(n_d = 1) = \frac{P(n_d \geq 1)}{1 + P(n_d \geq 1)}. \tag{3.8}$$

After optimizing the temperature of SHG, the dark counts are very low so in the subsequent discussion I neglect the dark count contributions.

3.2.2 Single rates at the idler detector

With this model, for a binary threshold idler detector (i), the expected single counts per clock cycle are:

$$R_i^{bin} = \sum_{n=1}^{\infty} \frac{\mu^n}{(1+\mu)^{n+1}} (1 - (1 - \eta_i)^n) = \frac{\mu \eta_i}{1 + \mu \eta_i} \tag{3.9}$$

[2]Note that using the binomial expansion representation does not yield the true wavefunction because the coefficients do not give the correct probabilities for normalization. The true coefficients need to be calculated from each term in the complete expansion of $(c^\dagger + id^\dagger)^n$, preserving order of $c^\dagger$ and $d^\dagger$.

[3]Not to be confused with hypothetical dark photons in beyond-the-Standard-Model physics! By "dark" photon, I mean a photon that is registered by the detector from a noise source.

[4]Here, "registering" is in quotes because the PNR detector will still detect any number of "dark" photons per clock cycle, but in post-processing we can discard all the multi-"dark" photon events.

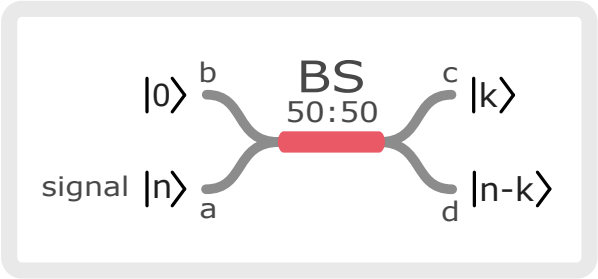

Figure 3.3: **Beamsplitter at Signal Arm**.
Input a connects to the signal arm output of the PBS,
output c is connects to the Signal 1 detector
and output d connects to the Signal 2 detector.

For a PNR idler detector (i) with unity PNR discrimination efficiency, the expected single counts per clock cycle are:

$$R_i^{pnr} = \sum_{n=1}^{\infty} \frac{\mu^n}{(1+\mu)^{n+1}} (\eta_i (1-\eta_i)^{n-1}) = \frac{\mu\eta_i}{(1+\mu)(1+\mu\eta_i)} \tag{3.10}$$

3.2.3 Single rates at the signal detectors

For a binary threshold signal detector (s_j where $j = 1, 2$), the expected single counts per clock cycle are:

$$R_{s_j}^{bin} = \sum_{n=1}^{\infty} \frac{\mu^n}{(1+\mu)^{n+1}} \sum_{k=1}^{n} \frac{\binom{n}{k}}{2^n} (1-(1-\eta_{s_j})^k) = \frac{\mu\eta_{s_j}}{2+\mu\eta_{s_j}} \tag{3.11}$$

3.2.4 Twofold Coincidence Rates

Without Dark Counts

The expected twofold coincidences per clock cycle for the two threshold signal detectors are:

$$\begin{aligned} R_{s_1,s_2}^{bin} &= \sum_{n=1}^{\infty} \frac{\mu^n}{(1+\mu)^{n+1}} \sum_{k=1}^{n-1} \frac{\binom{n}{k}}{2^n} (1-(1-\eta_{s_1})^k)(1-(1-\eta_{s_2})^{n-k}) \\ &= \frac{\mu^2\eta_{s_1}\eta_{s_2}(4+\mu(\eta_{s1}+\eta_{s_2}))}{(2+\mu\eta_{s_1})(2+\mu\eta_{s_2})(2+\mu(\eta_{s_1}+\eta_{s_2}))} \end{aligned} \tag{3.12}$$

For a binary threshold idler detector (i) and binary threshold signal detector (s_j where $j = 1, 2$), the expected twofold coincidences per clock cycle are:

$$\begin{aligned} R_{i,s_j}^{bin} &= \sum_{n=1}^{\infty} \frac{\mu^n}{(1+\mu)^{n+1}} (1-(1-\eta_i)^n) \sum_{k=1}^{n} \frac{\binom{n}{k}}{2^n} (1-(1-\eta_{s_j})^k) \\ &= \frac{\mu\eta_i}{1+\mu\eta_i} + \frac{2}{2-\mu\eta_i(\eta_{s_j}-2)+\mu\eta_{s_j}} - \frac{2}{2+\mu\eta_{s_j}} \end{aligned} \tag{3.13}$$

For a PNR idler detector (i) with unity PNR discrimination efficiency and binary threshold signal detector (s_j where $j = 1, 2$), the expected twofold coincidences per clock cycle are:

$$\begin{aligned} R_{i,s_j}^{pnr} &= \sum_{n=1}^{\infty} \frac{\mu^n}{(1+\mu)^{n+1}} (\eta_i(1-\eta_i)^{n-1}) \sum_{k=1}^{n} \frac{\binom{n}{k}}{2^n} (1-(1-\eta_{s_j})^k) \\ &= \frac{\mu\eta_i\eta_{s_j}}{(1+\mu\eta_i)(2-\mu\eta_i(\eta_{s_j}-2)+\mu\eta_{s_j})} \end{aligned} \tag{3.14}$$

3.2.5 Threefold Coincidence Rates

For a binary threshold idler detector (i) and binary threshold signal detectors (s_1, s_2), the expected threefold coincidences per clock cycle are:

$$\begin{aligned} R^{bin}_{i,s_1,s_2} &= \sum_{n=2}^{\infty} \frac{\mu^n}{(1+\mu)^{n+1}}(1-(1-\eta_i)^n) \sum_{k=1}^{n-1} \frac{\binom{n}{k}}{2^n}(1-(1-\eta_{s_1})^k)(1-(1-\eta_{s_2})^{n-k}) \\ &= 1 - \frac{1}{1+\mu\eta_i} - \frac{2}{2+\mu\eta_{s_1}} - \frac{2}{2+\mu\eta_{s_2}} + \frac{2}{2+\mu(\eta_{s_1}+\eta_{s_2})} \\ &+ \frac{2}{2-\mu\eta_i(\eta_{s_1}-2)+\mu\eta_{s_1}} + \frac{2}{2-\mu\eta_i(\eta_{s_2}-2)+\mu\eta_{s_2}} - \frac{2}{2(1+\mu\eta_i)+\mu(1-\eta_i)(\eta_{s_1}+\eta_{s_2})} \end{aligned} \tag{3.15}$$

For a PNR idler detector (i) with unity PNR discrimination efficiency and binary threshold signal detectors (s_1, s_2), the expected threefold coincidences per clock cycle are:

$$\begin{aligned} R^{pnr}_{i,s_1,s_2} &= \sum_{n=2}^{\infty} \frac{\mu^n}{(1+\mu)^{n+1}}(\eta_i(1-\eta_i)^{n-1}) \sum_{k=1}^{n-1} \frac{\binom{n}{k}}{2^n}(1-(1-\eta_{s_1})^k)(1-(1-\eta_{s_2})^{n-k}) \\ &= \frac{\mu\eta_i\eta_{s_1}}{(1+\mu\eta_i)(2(1+\mu\eta_i)+\mu\eta_{s_1}(1-\eta_i))} - \frac{2\mu\eta_i\eta_{s_1}}{(2(1+\mu\eta_i)+\mu\eta_{s_2}(1-\eta_i))(2(1+\mu\eta_i)+\mu(1-\eta_i)(\eta_{s_1}+\eta_{s_2}))} \end{aligned} \tag{3.16}$$

3.2.6 Calculating $g^{(2)}(0)$

The $g^{(2)}(0)$ correlation function is defined as:

$$g^{(2)}(0) = \frac{P(i,s_1,s_2)}{P(i,s_1)P(i,s_2)} \tag{3.17}$$

where $P(i,s_1,s_2) = R_{i,s_1,s_2}/R_i$ is the probability of threefold coincidences given a detection in the idler detector, $P(i,s_1) = R_{i,s_1}/R_i$ is the probability of twofold coincidences between the idler detector and signal detector 1, and $P(i,s_2) = R_{i,s_2}/R_i$ is the probability of twofold coincidences between the idler detector and signal detector 2. Substituting for $P(i,s_1,s_2)$, $P(i,s_1)$, and $P(i,s_2)$, the $g^{(2)}(0)$ function is:

$$g^{(2)}(0) = \frac{R_{i,s_1,s_2}R_i}{R_{i,s_1}R_{i,s_2}} \tag{3.18}$$

Equivalently, in terms of idler singles, twofold coincidences and threefold coincidences, the $g^{(2)}(0)$ function is:

$$g^{(2)}(0) = \frac{C_{i,s_1,s_2}C_i}{C_{i,s_1}C_{i,s_2}} \tag{3.19}$$

3.2.7 Measuring $g^{(2)}(0)$ from experiment

To experimentally determine the $g^{(2)}(0)$, we send single pulses at a clock rate (r) of 10^6 Hz and measure per second the single counts in each detector, the twofold coincidences, and the threefold coincidences.

Low μ

To leading order in R_i, R_{s_j}, R_{i,s_j} and R_{i,s_1,s_2},

$$C_i = rR_i = r\mu\eta_i \tag{3.20}$$

$$C_{s_j} = rR_{s_j} = r\mu\eta_{s_j}/2 \tag{3.21}$$

$$C_{i,s_j} = rR_{i,s_j} = r\mu\eta_i\eta_{s_j}/2 \tag{3.22}$$

$$C_{i,s_1,s_2} = rR_{i,s_1,s_2} = r\mu^2\eta_i(2-\eta_i)\eta_{s_2}\eta_{s_2}/2 \tag{3.23}$$

where C_i is the counts per second in the idler detector, C_{s_j} is the counts per second in signal detector j (where $j = 1,2$), C_{1,s_j} is the twofold coincidences per second between the idler detector and signal detector j, and C_{i,s_1,s_2} is the threefold coincidences per second of the idler and signal detectors.

For low μ (e.g. ≤ 0.1), we can calculate the idler efficiencies as

$$\eta_i = C_{i,s_j}/C_{s_j} \tag{3.24}$$

$$\eta_{s_j} = 2C_{i,s_j}/C_i \tag{3.25}$$

and μ as

$$\mu = \frac{C_i C_{s_j}}{r C_{i,s_j}} \tag{3.26}$$

Finally, we simply calculate the $g^{(2)}(0)$ according to (3.15).

Extracting μ, η_i, η_{s_1}, and η_{s_2} from single counts, twofold coincidences, and threefold coincidences

We can find true estimates for μ, η_i, η_{s_1}, and η_{s_2} by equating the single counts, twofold coincidences, and threefold coincidences to their respective equations of the model and finding the roots of the system of (nonlinear) equations. We end up with a system of six equations to solve for four variables. I write these equations in terms of the roots to solve for them numerically using the scipy optimize package.

For the ideal binary idler case, the root equations to solve for μ, η_i, η_{s_1}, and η_{s_2} are

$$0 = C_i^{bin} - \frac{r\mu\eta_i}{1+\mu\eta_i} \tag{3.27}$$

$$0 = C_{s_1} - \frac{r\mu\eta_{s_1}}{2+\mu\eta_{s_1}} \tag{3.28}$$

$$0 = C_{s_2} - \frac{r\mu\eta_{s_2}}{2+\mu\eta_{s_2}} \tag{3.29}$$

$$0 = C_{i,s_1}^{bin} - r\left(\frac{\mu\eta_i}{1+\mu\eta_i} + \frac{2}{2-\mu\eta_i(\eta_{s_1}-2)+\mu\eta_{s_1}} - \frac{2}{2+\mu\eta_{s_1}}\right) \tag{3.30}$$

$$0 = C_{i,s_2}^{bin} - r\left(\frac{\mu\eta_i}{1+\mu\eta_i} + \frac{2}{2-\mu\eta_i(\eta_{s_2}-2)+\mu\eta_{s_1}} - \frac{2}{2+\mu\eta_{s_2}}\right) \tag{3.31}$$

$$0 = C_{i,s_1,s_2}^{bin} - r\left(\frac{\mu\eta_i}{1+\mu\eta_i} - \frac{2}{2+\mu\eta_{s_1}} - \frac{2}{2+\mu\eta_{s_2}} + \frac{2}{2+\mu(\eta_{s_1}+\eta_{s_2})} + \right. \tag{3.32}$$
$$\left. \frac{2}{2-\mu\eta_i(\eta_{s_1}-2)+\mu\eta_{s_1}} + \frac{2}{2-\mu\eta_i(\eta_{s_2}-2)+\mu\eta_{s_2}} - \frac{2}{2(1+\mu\eta_i)+\mu(1-\eta_i)(\eta_{s_1}+\eta_{s_2})}\right)$$

For the ideal PNR idler case, the root equations to solve for μ, η_i, η_{s_1}, and η_{s_2} are

$$0 = C_i^{pnr} - \frac{r\mu\eta_i}{(1+\mu)(1+\mu\eta_i)} \tag{3.33}$$

$$0 = C_{s_1} - \frac{r\mu\eta_{s_1}}{2+\mu\eta_{s_1}} \tag{3.34}$$

$$0 = C_{s_2} - \frac{r\mu\eta_{s_2}}{2+\mu\eta_{s_2}} \tag{3.35}$$

$$0 = C_{i,s_1}^{pnr} - \frac{r\mu\eta_i\eta_{s_1}}{(1+\mu\eta_i)(2-\mu\eta_i(\eta_{s_1}-2)+\mu\eta_{s_1})} \tag{3.36}$$

$$0 = C_{i,s_2}^{pnr} - \frac{r\mu\eta_i\eta_{s_2}}{(1+\mu\eta_i)(2-\mu\eta_i(\eta_{s_2}-2)+\mu\eta_{s_2})} \tag{3.37}$$

$$0 = C_{i,s_1,s_2}^{pnr} - r\left(\frac{\mu\eta_i\eta_{s_1}}{(1+\mu\eta_i)(2(1+\mu\eta_i)+\mu\eta_{s_1}(1-\eta_i))} - \right. \tag{3.38}$$
$$\left. \frac{2\mu\eta_i\eta_{s_1}}{(2(1+\mu\eta_i)+\mu\eta_{s_2}(1-\eta_i))(2(1+\mu\eta_i)+\mu(1-\eta_i)(\eta_{s_1}+\eta_{s_2}))}\right)$$

3.3 Gaussian Model of $g^{(2)}(0)$ Experiment

From Sergio's SURF 2020 Interim Report II

All $\mathbb{I}_i$ are 2×2, the subscript refers to the mode. The probability that all three detectors click is given by:

$$Tr(\rho(\Pi_1 \otimes \Pi_2 \otimes \Pi_3)) = Tr(\rho((\mathbb{I}_1 - |0\rangle\langle 0|_1) \otimes (\mathbb{I}_2 - |0\rangle\langle 0|_2) \otimes (\mathbb{I}_3 - |0\rangle\langle 0|_3))).$$

Expanding and simplifying gives:

$$Tr(\rho(\mathbb{I}_{123} - \mathbb{I}_{12} \otimes |0\rangle\langle 0|_3 - \mathbb{I}_1 \otimes |0\rangle\langle 0|_2 \otimes \mathbb{I}_3 + \mathbb{I}_1 \otimes |0\rangle\langle 0|_{23} - |0\rangle\langle 0|_1 \otimes \mathbb{I}_{23} + |0\rangle\langle 0| \otimes \mathbb{I}_2 \otimes |0\rangle\langle 0|_3 + |0\rangle\langle 0|_{12} \otimes \mathbb{I}_3 - |0\rangle\langle 0|_{123}).$$

Now by linearity of trace, this is just:

$$\begin{aligned} &Tr(\rho) - Tr(\rho\,|0\rangle\langle 0|_1 \otimes \mathbb{I}_{23}) - Tr(\rho\mathbb{I}_1 \otimes |0\rangle\langle 0|_2 \otimes \mathbb{I}_3) - Tr(\rho\mathbb{I}_{2,3} \otimes |0\rangle\langle 0|_3) \\ &+ Tr(\rho\mathbb{I}_1 \otimes |0\rangle\langle 0|_{23}) + Tr(\rho\,|0\rangle\langle 0|_1 \otimes \mathbb{I}_2 \otimes |0\rangle\langle 0|_3) + Tr(\rho\,|0\rangle\langle 0|_{12} \otimes \mathbb{I}_3) - Tr(\rho\,|0\rangle\langle 0|_{123}) \end{aligned}$$

All that remains is to solve the remaining 7 integrals ($Tr(\rho) = 1$ is trivial).

First we need to find the covariance matrix γ of ρ. The initial state generated by SPDC is $|\psi\rangle = |TMSV\rangle$, which we know has the following covariance matrix.

$$\gamma_1 = \begin{pmatrix} 2\mu+1 & 0 & 2\sqrt{\mu(\mu+1)} & 0 \\ 0 & 2\mu+1 & 0 & -2\sqrt{\mu(\mu+1)} \\ 2\sqrt{\mu(\mu+1)} & 0 & 2\mu+1 & 0 \\ 0 & -2\sqrt{\mu(\mu+1)} & 0 & 2\mu+1 \end{pmatrix}$$

We consider the state $|0\rangle_1 |TMSV\rangle_{23}$ and will mix the vacuum mode with mode 2 of the TMSV state. The covariance matrix of this state is

$$\gamma_1' = \mathbb{I} \oplus \gamma_1 = \begin{pmatrix} 1 & 0 & 0 & 0 & 0 & 0 \\ 0 & 1 & 0 & 0 & 0 & 0 \\ 0 & 0 & 2\mu+1 & 0 & 2\sqrt{\mu(\mu+1)} & 0 \\ 0 & 0 & 0 & 2\mu+1 & 0 & -2\sqrt{\mu(\mu+1)} \\ 0 & 0 & 2\sqrt{\mu(\mu+1)} & 0 & 2\mu+1 & 0 \\ 0 & 0 & 0 & -2\sqrt{\mu(\mu+1)} & 0 & 2\mu+1 \end{pmatrix}$$

The signal mode of the TMSV state get split by a beamsplitter into two modes, while the third mode is unaffected. We represent this by the beamsplitter unitary below.

$$S \oplus \mathbb{I} = \begin{pmatrix} \frac{1}{\sqrt{2}} & 0 & 0 & -\frac{1}{\sqrt{2}} & 0 & 0 \\ 0 & \frac{1}{\sqrt{2}} & \frac{1}{\sqrt{2}} & 0 & 0 & 0 \\ 0 & -\frac{1}{\sqrt{2}} & \frac{1}{\sqrt{2}} & 0 & 0 & 0 \\ \frac{1}{\sqrt{2}} & 0 & 0 & \frac{1}{\sqrt{2}} & 0 & 0 \\ 0 & 0 & 0 & 0 & 1 & 0 \\ 0 & 0 & 0 & 0 & 0 & 1 \end{pmatrix}$$

The resulting covariance matrix we call γ_2 and is given by:

$$\begin{pmatrix} \mu+1 & 0 & 0 & -\mu & 0 & \sqrt{2}\sqrt{\mu(\mu+1)} \\ 0 & \mu+1 & \mu & 0 & \sqrt{2}\sqrt{\mu(\mu+1)} & 0 \\ 0 & \mu & \mu+1 & 0 & \sqrt{2}\sqrt{\mu(\mu+1)} & 0 \\ -\mu & 0 & 0 & \mu+1 & 0 & -\sqrt{2}\sqrt{\mu(\mu+1)} \\ 0 & \sqrt{2}\sqrt{\mu(\mu+1)} & \sqrt{2}\sqrt{\mu(\mu+1)} & 0 & 2\mu+1 & 0 \\ \sqrt{2}\sqrt{\mu(\mu+1)} & 0 & 0 & -\sqrt{2}\sqrt{\mu(\mu+1)} & 0 & 2\mu+1 \end{pmatrix}$$

Now we consider the loss in the channels. We do this by appending three vacuum modes (modes 4,5,6) to the state after the first beam splitter, then mixing each of the three relevant modes with its corresponding vacuum mode by using beamsplitters with transmittance of t_i, $i = 1, 2, 3$, then tracing out modes 4,5,6. The resulting covariance matrix is:

$$\begin{pmatrix} \eta_1\mu+2 & 0 & 0 & -\sqrt{\eta_1\eta_2}\mu & 0 & \sqrt{2\eta_1\eta_3\mu(\mu+1)} \\ 0 & \eta_1\mu+2 & \sqrt{\eta_1\eta_2}\mu & 0 & \sqrt{2\eta_1\eta_3\mu(\mu+1)} & 0 \\ 0 & \sqrt{\eta_1\eta_2}\mu & \eta_2\mu+2 & 0 & \sqrt{2\eta_2\eta_3\mu(\mu+1)} & 0 \\ -\sqrt{\eta_1\eta_2}\mu & 0 & 0 & \eta_2\mu+2 & 0 & -\sqrt{2\eta_2\eta_3\mu(\mu+1)} \\ 0 & \sqrt{2\eta_1\eta_3\mu(\mu+1)} & \sqrt{2\eta_2\eta_3\mu(\mu+1)} & 0 & 2\eta_3\mu+2 & 0 \\ \sqrt{2\eta_1\eta_3\mu(\mu+1)} & 0 & 0 & -\sqrt{2\eta_2\eta_3\mu(\mu+1)} & 0 & 2\eta_3\mu+2 \end{pmatrix}$$

What remains is to use this matrix to compute the trace integrals we saw above. This is done in the Mathematica file. We present the results below.

$$\begin{aligned}
Tr(\rho) &= 1 \\
Tr(\rho \left|0\right\rangle \left\langle 0\right|_1 \otimes \mathbb{I}_{23}) &= \frac{2}{2+\eta_1\mu} \\
Tr(\rho \mathbb{I}_1 \otimes \left|0\right\rangle \left\langle 0\right|_2 \otimes \mathbb{I}_3) &= \frac{2}{2+\eta_2\mu} \\
Tr(\rho \mathbb{I}_{23} \otimes \left|0\right\rangle \left\langle 0\right|_3) &= \frac{1}{1+\eta_3\mu} \\
Tr(\rho \left|0\right\rangle \left\langle 0\right|_{12} \otimes \mathbb{I}_3) &= \frac{2}{2+\eta_1\mu+\eta_2\mu} \\
Tr(\rho \left|0\right\rangle \left\langle 0\right|_1 \otimes \mathbb{I}_2 \otimes \left|0\right\rangle \left\langle 0\right|_3) &= \frac{2}{2+\eta_1\mu+2\eta_3\mu-\eta_1\eta_3\mu} \\
Tr(\rho \mathbb{I}_1 \otimes \left|0\right\rangle \left\langle 0\right|_{23}) &= \frac{2}{2+\eta_2\mu+2\eta_3\mu-\eta_2\eta_3\mu} \\
Tr(\rho \left|0\right\rangle \left\langle 0\right|_{123}) &= \frac{2}{2+\eta_1\mu+\eta_2\mu+2\eta_3\mu-\eta_1\eta_3\mu-\eta_2\eta_3\mu}
\end{aligned}$$

In fact, these calculations allow us to compute much more than just the three-fold coincidence count probability. We can also compute any single detector count probability and and two-fold coincidence count probabilities.

Single detector probabilities

The probability that detector 1 clicks is

$$Tr(\rho(\mathbb{I}_{123} - \left|0\right\rangle \left\langle 0\right|_1 \otimes \mathbb{I}_{23})) = 1 - \frac{2}{2+\eta_1\mu} = \frac{\eta_1\mu}{2+\eta_1\mu}.$$

Similarly, the probabilities that detectors 2 and 3 click are

$$Tr(\rho(\mathbb{I}_{123} - \mathbb{I}_1 \otimes \left|0\right\rangle \left\langle 0\right|_2 \otimes \mathbb{I}_3)) = \frac{\eta_2\mu}{2+\eta_2\mu}$$

and

$$Tr(\rho(\mathbb{I}_{123} - \mathbb{I}_{12} \otimes \left|0\right\rangle \left\langle 0\right|_3)) = \frac{\eta_3\mu}{1+\eta_3\mu},$$

respectively.

Two-fold detector count probabilities

The probability that detectors 1 and 2 click is

$$\begin{aligned}
Tr(\rho(\mathbb{I}_1 - \left|0\right\rangle \left\langle 0\right|_1)(\mathbb{I}_2 - \left|0\right\rangle \left\langle 0\right|_2)\mathbb{I}_3) &= 1 - \frac{2}{2+\eta_1\mu} - \frac{2}{2+\eta_2\mu} + \frac{2}{2+\eta_1\mu+\eta_2\mu} \\
&= \frac{\eta_1\eta_2\mu^2(4+\eta_1\mu+\eta_2\mu)}{(2+\eta_1\mu)(2+\eta_2\mu)(2+\eta_1\mu+\eta_2\mu)}.
\end{aligned}$$

Similarly, the probability that detectors 1 and 3 click is

$$Tr(\rho(\mathbb{I}_1 - \left|0\right\rangle \left\langle 0\right|_1)\mathbb{I}_2(\mathbb{I}_3 - \left|0\right\rangle \left\langle 0\right|_3)) = 1 - \frac{2}{2+\eta_1\mu} - \frac{1}{1+\eta_3\mu} + \frac{2}{2+\eta_1\mu+2\eta_3\mu-\eta_1\eta_3\mu},$$

and the probability that detectors 2 and 3 click is

$$Tr(\rho(\mathbb{I}_1(\mathbb{I}_2 - \left|0\right\rangle \left\langle 0\right|_2)(\mathbb{I}_3 - \left|0\right\rangle \left\langle 0\right|_3)) = 1 - \frac{2}{2+\eta_2\mu} - \frac{1}{1+\eta_3\mu} + \frac{2}{2+\eta_2\mu+2\eta_3\mu-\eta_2\eta_3\mu}.$$

Three-fold detector count probability

The probability that all three detectors click is given by the expression at the very top. Using all the results of our calculations, this is

$$
\begin{aligned}
&Tr(\rho) - Tr(\rho\left|0\right\rangle\left\langle 0\right|_1 \otimes \mathbb{I}_{23}) - Tr(\rho\mathbb{I}_1 \otimes \left|0\right\rangle\left\langle 0\right|_2 \otimes \mathbb{I}_3) - Tr(\rho\mathbb{I}_{2,3} \otimes \left|0\right\rangle\left\langle 0\right|_3) \\
&+ Tr(\rho\mathbb{I}_1 \otimes \left|0\right\rangle\left\langle 0\right|_{23}) + Tr(\rho\left|0\right\rangle\left\langle 0\right|_1 \otimes \mathbb{I}_2 \otimes \left|0\right\rangle\left\langle 0\right|_3) + Tr(\rho\left|0\right\rangle\left\langle 0\right|_{12} \otimes \mathbb{I}_3) - Tr(\rho\left|0\right\rangle\left\langle 0\right|_{123}) \\
&= 1 - \frac{2}{2+\eta_1\mu} - \frac{2}{2+\eta_2\mu} - \frac{1}{1+\eta_3\mu} + \frac{2}{2+\eta_1\mu+\eta_2\mu} + \frac{2}{2+\eta_1\mu+2\eta_3\mu-\eta_1\eta_3\mu} + \frac{2}{2+\eta_2\mu+2\eta_3\mu-\eta_2\eta_3\mu} \\
&- \frac{2}{2+\eta_1\mu+\eta_2\mu+2\eta_3\mu-\eta_1\eta_3\mu-\eta_2\eta_3\mu}
\end{aligned}
$$

3.3.1 Modeling with additional thermal modes

Schmidt decomposition

$$|\Psi\rangle = \sum_m \sqrt{\lambda_m} A^\dagger B^\dagger |00\rangle \tag{3.39}$$

We can get the λ_m's for different modes through singular value decomposition of the JSI. [23]

Joint Spectral Intensity (JSI)

Without spectral filtering [23]:

$$
\begin{aligned}
f(\nu_s, \nu_i) &= A(\omega_p = \omega_s + \omega_i) \\
&= M \exp\left[-\frac{\nu_s^2+\nu_i^2}{2\sigma^2} - \frac{2\nu_s\nu_i}{2\sigma^2}\right]
\end{aligned} \tag{3.40}
$$

With spectral filtering [23]:

$$f(\nu_s, \nu_i) = A \exp\left[-\frac{\nu_s^2+\nu_i^2}{2\sigma^2} - \frac{2\nu_s\nu_i}{2\sigma^2}\right] \exp\left[-\frac{\nu_s^2}{2\sigma_f^2}\right] \exp\left[-\frac{\nu_i^2}{2\sigma_f^2}\right] \tag{3.41}$$

$$\frac{1}{K} = \sqrt{1 - \frac{1}{\left(1 + \left(\frac{\sigma}{\sigma_f}\right)^2\right)^2}} \tag{3.42}$$

Introducing thermal modes

$$
\begin{aligned}
Tr(\rho) &= 1 \\
Tr(\rho\left|0\right\rangle\left\langle 0\right|_1 \otimes \mathbb{I}_{23}) &= \prod_m \frac{2}{2+\eta_1\lambda_m\mu} \\
Tr(\rho\mathbb{I}_1 \otimes \left|0\right\rangle\left\langle 0\right|_2 \otimes \mathbb{I}_3) &= \prod_m \frac{2}{2+\eta_2\lambda_m\mu} \\
Tr(\rho\mathbb{I}_{23} \otimes \left|0\right\rangle\left\langle 0\right|_3) &= \prod_m \frac{1}{1+\eta_3\lambda_m\mu} \\
Tr(\rho\left|0\right\rangle\left\langle 0\right|_{12} \otimes \mathbb{I}_3) &= \prod_m \frac{2}{2+\eta_1\lambda_m\mu+\eta_2\lambda_m\mu} \\
Tr(\rho\left|0\right\rangle\left\langle 0\right|_1 \otimes \mathbb{I}_2 \otimes \left|0\right\rangle\left\langle 0\right|_3) &= \prod_m \frac{2}{2+\eta_1\lambda_m\mu+2\eta_3\lambda_m\mu-\eta_1\eta_3\mu} \\
Tr(\rho\mathbb{I}_1 \otimes \left|0\right\rangle\left\langle 0\right|_{23}) &= \prod_m \frac{2}{2+\eta_2\lambda_m\mu+2\eta_3\lambda_m\mu-\eta_2\eta_3\lambda_m\mu} \\
Tr(\rho\left|0\right\rangle\left\langle 0\right|_{123}) &= \prod_m \frac{2}{2+\eta_1\lambda_m\mu+\eta_2\lambda_m\mu+2\eta_3\lambda_m\mu-\eta_1\eta_3\lambda_m\mu-\eta_2\eta_3\lambda_m\mu}
\end{aligned}
$$

3.3.2 Conclusion

Modeling the $g^{(2)}(0)$ experiment with a threshold using the Gaussian formalism agrees with discrete approach described in the previous section. The Gaussian formalism approach is a cleaner way to encompass full multiphoton effects of the experiment. However, we cannot immediately model the experiment in the PNR idler detector case because the PNR measurement operator is not a Gaussian operator.

Is there a way to model a PNR detector in the Gaussian formalism using a series of Gaussian operators (e.g. linear optics and threshold detectors)? I answer this question in the next section by looking for inspiration in proposed PNR detector models, such as the 2N-Port beamsplitter model.

3.4 Gaussian Modeling of PNR detectors

3.4.1 2N-Port Beamsplitter Model

In [11], Paul et al. propose a method of using a $2N$-port beam splitter to measure photon number distribution of the pure quantum state of a single-mode light field. They consider a state $|\psi\rangle = \sum_{n=0}^{\infty} c_n |n\rangle$ incident on a single input of a $2N$-port beam splitter, depicted in figure 3.4.

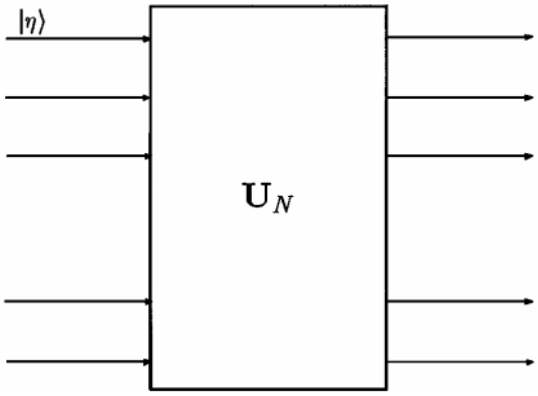

.

Figure 3.4: **2N-Port Beamsplitter** with $N = 2^k$ inputs and outputs.

Consider a set of N threshold detectors, one at each output of the beamsplitter. When a single photon is fed into the first input of the beamsplitter (with vacuum modes at each of the $N-1$ inputs), the beamsplitter acts to "split" the photon into an equal superposition of the N output modes. As such, an arbitrary Fock state $|n\rangle$ transforms as

$$U_N |n\rangle = U_N \frac{1}{\sqrt{n!}} \left(\hat{a_1}^\dagger\right)^n |0\rangle = \frac{1}{\sqrt{n!}} \frac{1}{(\sqrt{N})^n} \left(\sum_{i=1}^{N} \hat{b_i}^\dagger\right)^n |0\rangle \tag{3.43}$$

where $\hat{a_i}^\dagger$ and $\hat{b_i}^\dagger$ are the creation operators for the ith input and output modes, respectively. Here, $1/\sqrt{n!}$ is the normalization constant for the creation operator and the $1/\sqrt{N}$ accounts for the equal probability of a single photon over each output mode.

Since $\hat{b}_i^\dagger$ form a set of commuting operators, the multinomial theorem states that

$$\left(\sum_{i=1}^{N} \hat{b_i}^\dagger\right)^n = \sum_{j_1+j_2+\ldots+j_N=n} \frac{n!}{j_1!j_2!\ldots j_N!} \prod_{t=1}^{N} \left(\hat{b}_t^\dagger\right)^{j_t} \tag{3.44}$$

where the sum is taken over the set $\{j_j\}$ of all combinations of nonnegative j_1 through j_N in which $\sum j_j = n$. After applying the multinomial theorem and normalizing the coefficients, we get:

$$U_N |n\rangle = \frac{1}{(\sqrt{N})^n} \sum_{j_1+j_2+\ldots+j_N=n} \sqrt{\frac{n!}{j_1!j_2!\ldots j_N!}} |j_1\rangle |j_2\rangle \ldots |j_N\rangle \tag{3.45}$$

So the joint probability of finding j_1 photons at output 1, j_2 photons at output 2, ... , and j_N photons at output N is

$$P_n(j_1, j_2, ..., j_N) = \frac{1}{N^n} \frac{n!}{j_1! j_2! ... j_N!} \tag{3.46}$$

Now, the probability that n photons (at input 1) trigger m simultaneous clicks, where $m = 1, 2, ..., n$, is

$$P^N_{m,n} = \frac{n!}{N^n} \sum_{j_1+j_2+...+j_N=n}^{(m)} \frac{1}{j_1! j_2! ... j_N!} \tag{3.47}$$

where (m) refers to the condition that m of $\{j_i\}$ are nonzero, n still refers to the number of photons incident to input 1 and N denotes the number of input/output ports. To find the explicit form of $P^N_{m,n}$, Paul et al. invoke the following recursion relation:

$$P^N_{m,n} = P^N_{m,n-1} \frac{m}{N} + P^N_{m-1,n-1} \frac{N-(m-1)}{N} \tag{3.48}$$

I have modified the notation that [11] use in equation (9) (i.e. taking $n \to n-1$ and rearranging) for a more intuitive presentation: the probability that n input photons trigger m output ports ($P^N_{m,n}$) *equals* the probability that the first $n-1$ input photons trigger m output ports ($P^N_{m,n-1}$) *times* the probability that the nth input photon triggers one of the m already triggered outputs ($\frac{m}{N}$) *plus* the probability that the first $n-1$ input photons trigger $m-1$ outputs ($P^N_{m-1,n-1}$) *times* the probability that the nth photon triggers one of the $N-(m-1)$ "un-triggered" outputs ($\frac{N-(m-1)}{N}$). Putting together 3.47 and 3.48 yields equation (10) of [11]:

$$P^N_{m,n} = \frac{1}{N^n} \binom{N}{m} \sum_{i=0}^{m} (-1)^i \binom{m}{i} (m-i)^n \tag{3.49}$$

where $N \geq n \geq m$. Perhaps a more intuitive presentation of 3.49 is

$$P^N_{m,n} = \frac{m!}{N^n} \binom{N}{m} S(n, m) \tag{3.50}$$

where $S(n, m)$ is the Stirling Number of the second kind [21], which from number theory is the number of ways of partitioning a set of n elements into m non empty sets. In other words, $P^N_{m,n}$ is proportional to the number of ways of distributing n input photons over m output modes. Note that for $m > n$, $P^N_{m,n} = 0$ because there are no ways of distributing n photons over $m > n$ output modes.

3.4.2 2N-Port Beamsplitter as a PNR Detector

This scheme can be used to model photon number resolving (PNR) detectors using threshold detectors. An ideal PNR measures n photons when n photons are incident. Equivalently, the probability that the detector measures n photons equals the probability that Fock state $|n\rangle$ is incident to the detector. We can consider the 2N-port beamsplitter scheme as a PNR detector, where the PNR detection mechanism is the joint measurement of simultaneously triggered output mode detectors. In other words, an x-fold "coincidence" measurement of the N output mode detectors is a measurement of Fock state $|x\rangle$. For $N >> n$, the probability that any given output mode receives multiple photons is small, so we expect the number of simultaneously triggered detectors to be equal to the number of input photons as $N \to \infty$. In other words,

$$\lim_{N\to\infty} P^N_{m,n} = \delta_{m,n}$$

On the other hand, when N is small, there is a non-negligible probability that any given output mode receives more than one photon, such that the number of simultaneously triggered output detectors is less than the number of input photons. This gives an avenue for modeling PNR discrimination efficiency: there is some probability that the PNR detector will detect x input photons when there were in fact $n > x$ input photons. Figure 3.5 depicts series of plots of $P^N_{m,10}$ over m for $N = 8, 32, 128, 1024$ to show how discrimination efficiency improves with increasing N for input Fock state $|10\rangle$.

Many quantum optics experiments are interested in detectors that can discriminate between zero photons, one photon, and more than one photon. Experiments can use PNR detectors to filter out multiphoton noise that can severely limit e.g. quantum communication rates and fidelities by triggering the experiment on the measurements of single photons. To fully model these experiments, it is important

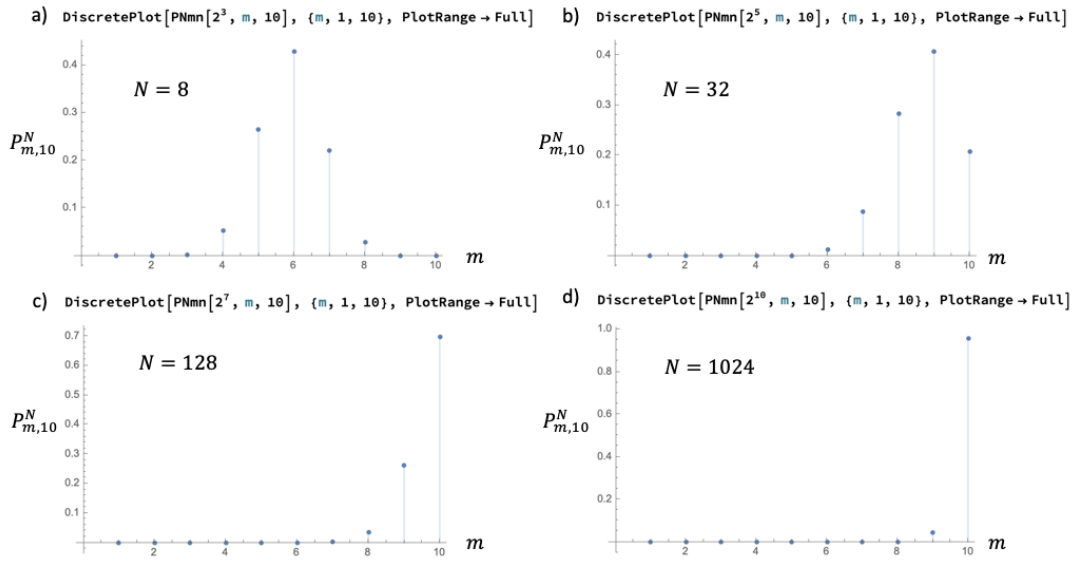

Figure 3.5: **Probability that m output detectors are triggered for ten input photons** versus m for $N = 8, 32, 128, 1024$

to know the probability $P^N_{1,n}$ of detecting a single photon given input state $|n\rangle$ to the detector. Figure 3.6 depicts a series of plots of $P^N_{1,n}$ over n for $N = 2, 8, 32, 1024$. The $N = 2$ case corresponds to a regular 50:50 beamsplitter, and we see that $P^2_{1,n}$ falls off as $1/2^n$ as expected.

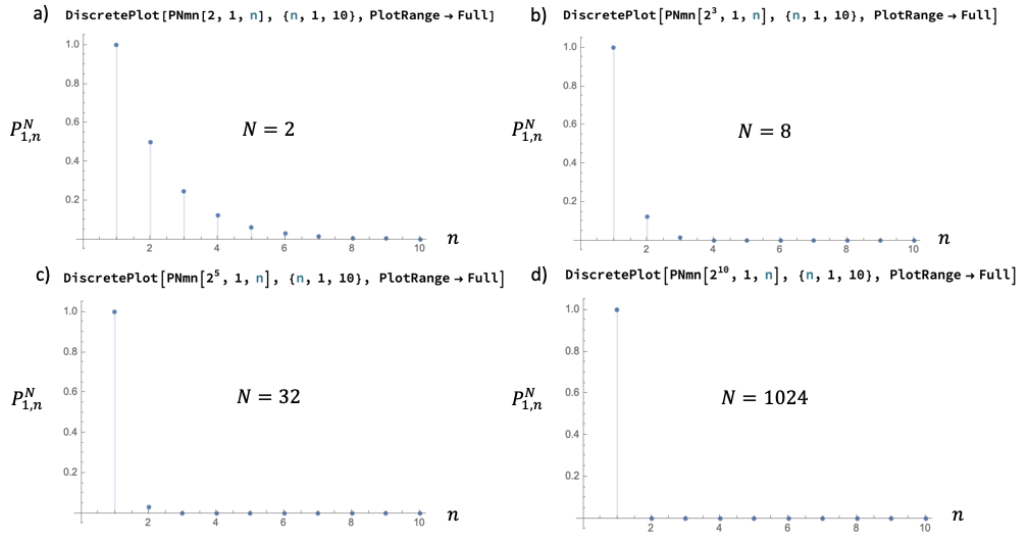

Figure 3.6: **Probability that one output detector is triggered for n input photons** versus n for $N = 2, 8, 32, 1024$

It follows that the probability that a perfect PNR detector measures a single photon is equal to the single photon probability of the input state: for input $|\psi\rangle = \sum_{n=0}^{\infty} c_n |n\rangle$, the probability of detecting a single photon is $|c_1|^2$.

3.4.3 Gaussian Formalism of the 2N-Port Beamsplitter Model of PNR Detectors

In the remainder of this work, I use the characteristic function formalism of [15] with the notation from [19] to study the transformation of quantum states incident to the system of N input modes of the 2N-port beamsplitter.

Gaussian Formalism

Consider an N-mode bosonic system associated with N pairs of annihilation and creation operators $\{\hat{a}_j, \hat{a}_j^\dagger\}_{j=1,...,N}$ that satisfy commutation relations $[\hat{a}_j, \hat{a}_k^\dagger] = \delta_{j,k}$. For each mode j, we construct the quadrature field operators as:

$$\hat{q}_j = \frac{1}{\sqrt{2}}\left(\hat{a}_j^\dagger + \hat{a}_j\right) \tag{3.51}$$

$$\hat{p}_j = \frac{i}{\sqrt{2}}\left(\hat{a}_j^\dagger - \hat{a}_j\right) \tag{3.52}$$

A quantum state with density operator $\hat{\rho}$ in the N-mode system is described by its characteristic function,

$$\chi(x) = Tr[\hat{\rho}\hat{W}(x)] \tag{3.53}$$

where

$$\hat{W}(x) = e^{-ix^T\hat{R}} \tag{3.54}$$

is a Weyl operator, $\hat{R} = [\hat{q}_1, \hat{p}_1, ..., \hat{q}_N, \hat{p}_N]^T$ is a 2N column vector of quadrature operators ($\hat{q}_j$, $\hat{p}_j$ for mode j), and $x = [x_{q_1}, x_{p_1}, ..., x_{q_N}, x_{p_N}]^T$ is 2N real column vector.

Gaussian states (e.g. vacuum state, coherent state, two-mode squeezed vacuum state) and operators (e.g. linear optics, threshold detectors) span a versatile set of states and components used in quantum optics experiments. A Gaussian state is defined as a quantum state with characteristic function of the form:

$$\chi(x) = e^{-\frac{1}{4}x^T\gamma x - id^T x} \tag{3.55}$$

where γ is a $2N$ by $2N$ matrix called the covariance matrix and d is a $2N$ column vector called the displacement vector. One important Gaussian state for SPDC experiments is the two-mode squeezed vacuum state (TMSV), which has covariance matrix (as a function of μ, the mean photon number per mode)

$$\gamma^{TMSV}(\mu) = \begin{pmatrix} 2\mu+1 & 0 & 2\sqrt{\mu(\mu+1)} & 0 \\ 0 & 2\mu+1 & 0 & -2\sqrt{\mu(\mu+1)} \\ 2\sqrt{\mu(\mu+1)} & 0 & 2\mu+1 & 0 \\ 0 & -2\sqrt{\mu(\mu+1)} & 0 & 2\mu+1 \end{pmatrix} \tag{3.56}$$

and displacement vector $d = 0$.

A Gaussian operator transforms a Gaussian state to another Gaussian state. Any Gaussian unitary operation on a Gaussian state can be described by symplectic transformations of the covariance matrix and displacement vector of the form:

$$\gamma \to S\gamma S^T \tag{3.57}$$

$$d \to Sd \tag{3.58}$$

For example, the symplectic matrix of the 50:50 beamsplitter in our notation is:

$$S^{\text{BS}} = \begin{pmatrix} \frac{1}{\sqrt{2}} & 0 & 0 & -\frac{1}{\sqrt{2}} \\ 0 & -\frac{1}{\sqrt{2}} & \frac{1}{\sqrt{2}} & 0 \\ \frac{1}{\sqrt{2}} & 0 & 0 & \frac{1}{\sqrt{2}} \end{pmatrix} \tag{3.59}$$

Given the covariance matrix of a Gaussian state, we can calculate several important experimental values including rates and fidelities. The most important for our purposes is the probability that a threshold photon detector registers a photon. For a measurement device with measurement operator $\hat{\Pi}$, the probability of detecting state ρ is:

$$Tr[\hat{\rho}\hat{\Pi}] = \left(\frac{1}{2\pi}\right)^n \int dx \chi_\rho(x)\chi_\Pi(-x) \tag{3.60}$$

For threshold detectors, which discriminate between only zero and non-zero photons, the "on" and "off" measurement operators are:

$$\hat{\Pi}_{\text{off}} = |0\rangle\langle 0| \tag{3.61}$$

$$\hat{\Pi}_{\text{on}} = \hat{I} - |0\rangle\langle 0| \tag{3.62}$$

Let $\hat{\rho}$ be a single-mode Gaussian state with displacement vector $d = 0$ and characteristic function $\chi_\rho(x) = e^{-\frac{1}{4}x^T\gamma x}$. Then the probability of detecting zero photons simplifies to

$$P_{\text{off}} = Tr[\hat{\rho}\hat{\Pi}_{\text{off}}] = Tr[\hat{\rho}\,|0\rangle\langle 0|] = \frac{2}{\sqrt{\det(\gamma + I)}} \tag{3.63}$$

and the probability of detecting non-zero photons is

$$P_{\text{on}} = Tr[\hat{\rho}\hat{\Pi}_{\text{on}}] = 1 - Tr[\hat{\rho}\,|0\rangle\langle 0|] = 1 - \frac{2}{\sqrt{\det(\gamma + I)}} \tag{3.64}$$

We will need to calculate the probability of coincidence photon counts across multiple modes of an N mode state. Suppose we have a threshold detector at each of the N modes, and we want to calculate the probability of detecting non-zero photons at m of the modes (an "m-fold coincidence"). Then the probability of an m-fold coincidence for an N-mode Gaussian state with covariance matrix γ_N is:

$$\sum_{\{m\}} Tr[\hat{\rho}^{\gamma_N}(\hat{\Pi}_{\text{on}}^{\otimes m} \otimes \hat{\Pi}_{\text{off}}^{\otimes(N-m)})] = \sum_{\{m\}} Tr[\hat{\rho}^{\gamma_N}((\hat{I} - |0\rangle\langle 0|)^{\otimes m} \otimes |0\rangle\langle 0|^{\otimes(N-m)})] \tag{3.65}$$

where $\sum_{\{m\}}$ indicates a sum over the all possible choices of m output modes. This results in a linear combination of $\binom{N}{m}$ terms of the form,

$$Tr[\hat{\rho}^{\gamma_N}(\hat{I}^{\otimes k} \otimes |0\rangle\langle 0|^{\otimes(N-k)})] = Tr[\hat{\rho}_{\text{red}}^{\gamma_N}\,|0\rangle\langle 0|^{\otimes(N-k)}] \tag{3.66}$$

which is a partial trace of $\hat{\rho}_N^{\gamma}$ over $N-k$ modes where $0 \le k \le N$. One useful property of Gaussian states is that the covariance matrix of the reduced state after a partial trace is just the submatrix corresponding to the remaining system. It can be shown that for a N-mode system with covariance matrix γ_N and displacement vector d_N, the probability of measuring zero photons across the n modes is:

$$Tr[\hat{\rho}\hat{\Pi}_{\text{off}}^{\otimes N}] = Tr[\hat{\rho}\,|0\rangle\langle 0|^{\otimes n}] = \frac{2^N}{\sqrt{\det(\gamma_N + I_N)}} e^{-d_N^T(\gamma_N + I_N)^{-1}d_N} \tag{3.67}$$

So, (3.66) simplifies to

$$Tr[\hat{\rho}_{\text{red}}^{\gamma_N}\,|0\rangle\langle 0|^{\otimes(N-k)}] = \frac{2^{N-k}}{\sqrt{\det(\gamma_{N-k} + I_{N-k})}} e^{-d_{N-k}^T(\gamma_{N-k} + I_{N-k})^{-1}d_{N-k}} \tag{3.68}$$

where I_m is the m by m identity matrix, γ_{N-k} is the submatrix of γ_N and d_{N-k} is the sub vector of d_N corresponding to the remaining subsystem of $N-k$ modes. By knowing γ_N and d_N of the full N mode system, we can find the m-fold coincidence probability for arbitrary m, where $0 \le m \le N$.

PNR Detector as a Gaussian Operator

Suppose we find a Gaussian operator construction of a 2N-port beamsplitter and use this to model a PNR detector. For a single mode Gaussian input state $\hat{\rho}^{\gamma}$ with covariance matrix γ, we want to find the probability of measuring m photons, i.e. the probability of an m-fold coincidence in the output modes of the 2N-port beamsplitter. First we have to convert single mode covariance matrix γ into the N-mode covariance matrix γ_N by appending $N-1$ vacuum modes to γ. If $\hat{\rho}$ is incident to input mode j, then γ_N is:

$$\gamma_N = I^{\oplus j-1} \oplus \gamma \oplus I^{\oplus N-j-1} \tag{3.69}$$

From (3.65) and (3.57), we get:

$$Tr[\hat{\rho}^{\gamma'_N}(\hat{\Pi}_{\text{on}}^{\otimes m} \otimes \hat{\Pi}_{\text{off}}^{\otimes(N-m)})] = Tr[\hat{\rho}^{\gamma'_N}((\hat{I} - |0\rangle\langle 0|)^{\otimes m} \otimes |0\rangle\langle 0|^{\otimes(N-m)})] \tag{3.70}$$

where $\rho^{\gamma'_N}$ is the output state with covariance matrix $\gamma'_N = S\gamma_N S^T$ and S is the symplectic matrix of the 2N-port beamsplitter.

Most quantum communication protocols only need to discriminate between zero, one, and more than one photons. The multiphoton events are discarded in these applications, so we are only interested in

the single photon detection probability P_1^N of the PNR detector. We model this as the probability that a single output mode of the 2N-port beamsplitter is turned on:

$$P_1^N = NTr[\hat{\rho}^{\gamma'_N}(\hat{\Pi}_{\text{on}} \otimes \hat{\Pi}_{\text{off}}^{\otimes(N-1)})] = Tr[\hat{\rho}^{\gamma'_N}((\hat{I} - |0\rangle\langle 0|) \otimes |0\rangle\langle 0|^{\otimes(N-1)})] \tag{3.71}$$

$$= NTr[\hat{\rho}^{\gamma'_N}(\hat{I} \otimes |0\rangle\langle 0|^{\otimes(N-1)})] - NTr[\hat{\rho}^{\gamma'_N}|0\rangle\langle 0|^{\otimes N}] \tag{3.72}$$

$$= \frac{N2^{N-1}}{\sqrt{\det(\gamma'_{N-1} + I_{N-1})}} e^{-d'_{N-1}{}^T(\gamma'_N + I_{N-1})^{-1} d_{N-1}} - \frac{N2^N}{\sqrt{\det(\gamma'_N{}' + I_N)}} e^{-d'_N{}^T(\gamma'_N + I_N)^{-1} d'_N} \tag{3.73}$$

As $N \to \infty$, we expect the 2N-port model to approach a PNR detector with perfect discrimination efficiency, such that the single photon detection probability equals the single photon probability of the input state.

$$\lim_{N\to\infty} P_1^N = \langle 1|\rho^{\gamma'_N}|1\rangle \tag{3.74}$$

More generally, we expect the probability of m-fold coincidences P_m^N to approach the m-photon probability of the input state for large N:

$$\lim_{N\to\infty} P_m^N = \langle m|\rho^{\gamma'_N}|m\rangle \tag{3.75}$$

Since P_m^N is a function of S, in order use the 2N-port beamsplitter to model a PNR detector in the Gaussian formalism, we need to find the corresponding symplectic matrix.

Finding a Gaussian Operator Construction of the 2N-Port Beamsplitter

Our task is to create a 2N-port beamsplitter that is a Gaussian operator. We want to construct a 2N-port beamsplitter out of a series of Gaussian transformations that distributes photons incident to *some* input mode over an equal superposition of the output modes. One possible construction is a binary tree of 50:50 beamsplitters, where $N = 2^k$ is the number of input/output modes and k denotes the "order" (i.e. depth) of the tree (Figure 3.7).

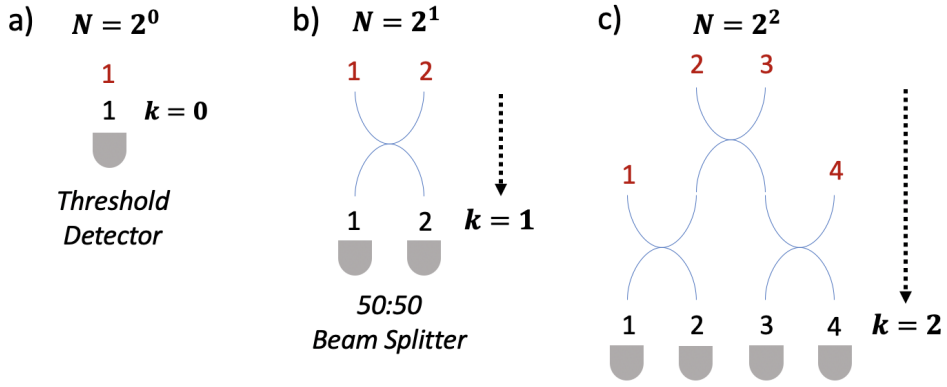

Figure 3.7: **Binary Trees of 50:50 Beamsplitters** as 2N-Port Beamsplitter. The red numbers denote the N input modes and black numbers denote the N output modes.

There are a few important observations to make about the binary tree construction. First, for a tree of order k, there are always $N = 2^k$ input modes and output modes. Second, a photon that enters either of the two input modes of the *top* beamsplitter (e.g. modes 2,3 for k=2), for any order tree, will have an equal probability of appearing at each output mode (provided that the beamsplitters are exactly 50:50). Conversely, a photon that enters any of the other input modes will *not* have an equal probability of appearing at each output mode. So it is important the keep track of which input modes correspond to the top beamsplitter, because it is only when photons are incident to these modes that the binary tree is a valid construction of the 2N-port beamsplitter. Third, the binary tree is *recursive*: to construct a binary tree of order $k+1$, take two binary trees of order k, choose one of the two top-most input modes from each tree, and input each mode into a 50:50 beamsplitter.

Finding the Symplectic Matrix of a Binary Tree of Beamsplitters

Now the goal is to find the symplectic matrix S_k of an arbitrary binary tree of order k. We will take advantage of the recursive symmetry of the binary tree to find a pattern for calculating S_k.

First, consider the characteristic function of a state with covariance matrix γ and displacement vector $d = 0$ after a Gaussian transformation. We can interpret S acting on x, transforming $\chi(x) \to \chi(x')$ where $x' = Sx$:

$$\chi(x) = e^{-\frac{1}{4}x^T\gamma x} \to e^{-\frac{1}{4}x^T S^T\gamma Sx} = e^{-\frac{1}{4}x'^T\gamma x'} = \chi(x') \tag{3.76}$$

I will simplify our notation by grouping together the elements corresponding to individual nodes, taking $(x_{q_i}, x_{p_i}) \to \vec{x}_i$. This changes the representation of S from a $2N$ by $2N$ matrix to N by N matrix and the representations of x and d from column vectors of length $2N$ to column vectors of length N. Now we may think of x as a column vector representation of the N input modes, x' as a column vector representation of the N output modes, and S as carrying out the operation of the 2N-port beamsplitter on the input modes (Figure 3.8).

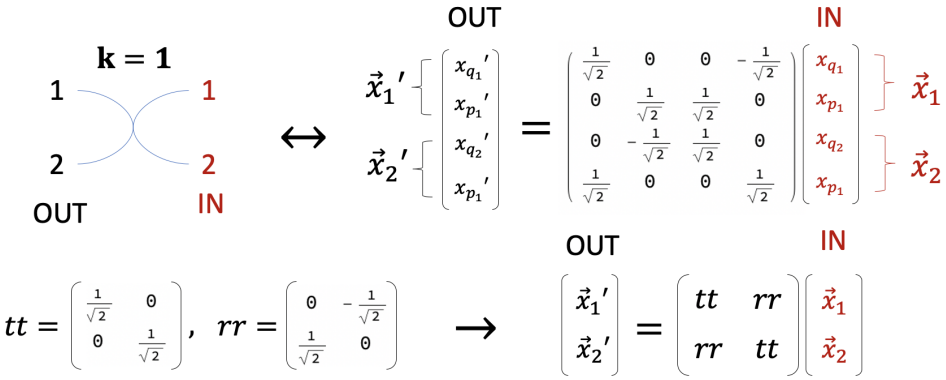

Figure 3.8: **Symplectic Matrix (S_1) for a 50:50 Beamsplitter** i.e. a k=1 binary tree.

With this picture in mind, we find the following recursive construction of the symplectic matrix, depicted in Figure 3.9.

$$S_k = S_1^{o\oplus 2^{k-1}} \cdot S_2^{o\oplus 2^{k-2}} \cdots S_{k-1}^{o\oplus 2} \cdot S_k^o = \Pi_{i=1}^k S_i^{o\oplus 2^{k-i}} \tag{3.77}$$

$$= (S_{k-1} \oplus S_{k-1}) S_k^o \tag{3.78}$$

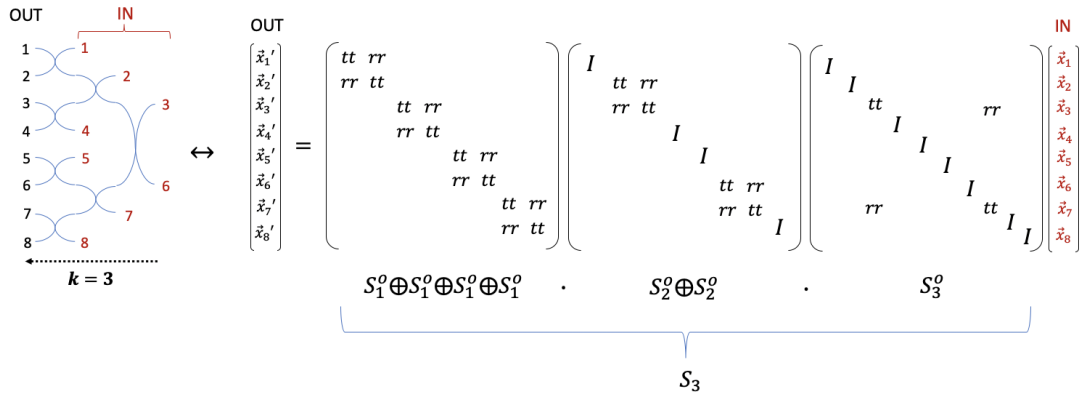

Figure 3.9: **Symplectic Matrix Construction for a Binary Tree of order k=3**

This construction is depicted in Figure 3.9 and reflects recursive construction of the binary tree: to make S_k, concatenate two S_{k-1}'s and apply S_k^o, a 2-port beamsplitter symplectic matrix to the top-most inputs of the trees of order $k-1$ (Figure 3.10).

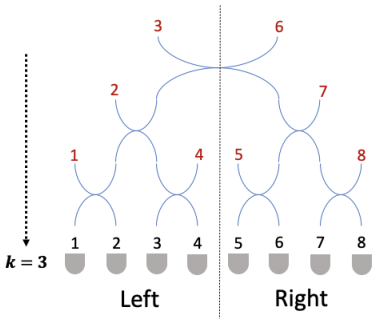

$$S_3^o = \begin{pmatrix} I & & & & & & & \\ & I & & & & & & \\ & & tt & & & & rr & \\ & & & I & & & & \\ & & & & I & & & \\ & & & & & I & & \\ & & rr & & & & tt & \\ & & & & & & & I \\ & & & & & & & & I \end{pmatrix}$$

k	Left Index (l_k)	Right Index (r_k)
1	1	2
2	2	3
3	3	6
4	6	11
5	11	22
k	r_{k-1}	$2^k - r_{k-1} + 1$

$$l_k = r_{k-1} \qquad r_k = 2^k - l_k + 1$$

$$S_k^o = A_{n,m}$$

$$= \begin{cases} tt & \text{if } n = m = l_k \text{ or } r_k \\ rr & \text{if } n, m = l_k, r_k \text{ or } r_k, l_k \\ I & \text{if } n = m \neq l_k \text{ or } r_k \\ 0 & \text{otherwise} \end{cases}$$

Figure 3.10: **Recursive Formula for** S_k^o. In this notation, l_k is the index of the left top-most input, r_k is the index of the left top-most input, and $A_{n,m}$ is the (n,m) matrix element of S_k^o for a tree of order k. The input state *must* be incident to input modes l_k or r_k.

3.4.4 Thermal state incident to a Binary Tree of Beamsplitters

To test this model, I calculate the single photon probability, twofold probability, and threefold probability of a thermal state incident to the binary tree. I expect that as I increase the order k of the tree, the probabilities converge to the single photon, two photon, and three photon probabilities of the thermal state (i.e. the square of the respective amplitudes of the thermal state in the Fock basis expansion, P_n^{th}). A thermal state is defined as

$$\rho^{th} = \sum_{n=0}^{\infty} P_n^{th} |n\rangle \langle n| = \sum_{n=0}^{\infty} \frac{\mu^n}{(1+\mu)^{n+1}} |n\rangle \langle n| \tag{3.79}$$

so I expect to find $P_1^{th} = \frac{\mu}{(1+\mu)^2}$, $P_2^{th} \frac{\mu^2}{(1+\mu)^3}$, and $P_3^{th} = \frac{\mu^3}{(1+\mu)^4}$ for large k.

```
Table[Simplify[Pmk[idlerCovIdeal, {0, 0}, k, 2], {μ > 0, n > 0}], {k, 7}]
```

$$\left\{\frac{2\,\mu}{2+3\,\mu+\mu^2}, \frac{4\,\mu}{4+7\,\mu+3\,\mu^2}, \frac{8\,\mu}{8+15\,\mu+7\,\mu^2}, \frac{16\,\mu}{16+31\,\mu+15\,\mu^2}, \frac{32\,\mu}{32+63\,\mu+31\,\mu^2}, \frac{64\,\mu}{(1+\mu)\,(64+63\,\mu)}, \frac{128\,\mu}{(1+\mu)\,(128+127\,\mu)}\right\}$$

Figure 3.11: **Single Coincidence Probability of Thermal State** for k-order trees from $k = 1$ to $k = 7$.

By calculating P_1^k for trees of order $k = 1$ to $k = 7$, I deduce the general expression of P_1^k:

$$P_1^k = \frac{2^k \mu}{(1+\mu)(2^k + (2^k - 1)\mu)} \tag{3.80}$$

Taking the limit of $k \to \infty$, we recover P_1^{th}.

$$\lim_{k\to\infty} \frac{2^k \mu}{(1+\mu)(2^k + (2^k - 1)\mu)} = \frac{\mu}{(1+\mu)^2} = P_1^{th} \tag{3.81}$$

```
Table[Simplify[Pmk2[idlerCovIdeal, {0, 0}, k, 1], {μ > 0, n > 0}], {k, 7}]
```

$$\left\{\frac{\mu^2}{2+3\,\mu+\mu^2}, \frac{6\,\mu^2}{8+18\,\mu+13\,\mu^2+3\,\mu^3}, \frac{28\,\mu^2}{32+84\,\mu+73\,\mu^2+21\,\mu^3}, \frac{120\,\mu^2}{(1+\mu)\,(8+7\,\mu)\,(16+15\,\mu)}, \frac{496\,\mu^2}{(1+\mu)\,(16+15\,\mu)\,(32+31\,\mu)}, \frac{2016\,\mu^2}{(1+\mu)\,(32+31\,\mu)\,(64+63\,\mu)}, \frac{8128\,\mu^2}{(1+\mu)\,(64+63\,\mu)\,(128+127\,\mu)}\right\}$$

Figure 3.12: **Two-fold Coincidence Probability of Thermal State** for k-order trees from $k = 1$ to $k = 7$.

By calculating P_2^k for trees of order $k = 1$ to $k = 7$, I deduce the general expression of P_2^k:

$$P_2^k = \frac{2^{k-1}(2^k - 1)\mu^2}{(1+\mu)(2^{k-1} + (2^{k-1} - 1)\mu)(2^k + (2^k - 1)\mu)} \tag{3.82}$$

Taking the limit of $k \to \infty$, we recover P_2^{th}.

$$\lim_{k\to\infty} \frac{2^{k-1}(2^k - 1)\mu^2}{(1+\mu)(2^{k-1} + (2^{k-1} - 1)\mu)(2^k + (2^k - 1)\mu)} = \frac{\mu^2}{(1+\mu)^3} = P_2^{th} \tag{3.83}$$

```
Table[Simplify[Pmk3[idlerCovIdeal, {0, 0}, k, 1], {μ > 0, n > 0}], {k, 7}]
```

$$\left\{0, 4\,\mu\left(\frac{1}{1+\mu} - \frac{6}{8+10\,\mu+3\,\mu^2}\right), \frac{168\,\mu^3}{(1+\mu)\,(4+3\,\mu)\,(8+5\,\mu)\,(8+7\,\mu)}, \frac{1680\,\mu^3}{(1+\mu)\,(8+7\,\mu)\,(16+13\,\mu)\,(16+15\,\mu)},\right.$$
$$\left.\frac{14\,880\,\mu^3}{(1+\mu)\,(16+15\,\mu)\,(32+29\,\mu)\,(32+31\,\mu)}, \frac{124\,992\,\mu^3}{(1+\mu)\,(32+31\,\mu)\,(64+61\,\mu)\,(64+63\,\mu)}, \frac{1\,024\,128\,\mu^3}{(1+\mu)\,(64+63\,\mu)\,(128+125\,\mu)\,(128+127\,\mu)}\right\}$$

Figure 3.13: **Three-fold Coincidence Probability of Thermal State** for k-order trees from $k = 1$ to $k = 7$.

By calculating P_3^k for trees of order $k = 1$ to $k = 7$, I deduce the general expression of P_3^k:

$$P_3^k = \frac{(2^{k-1} - 1)2^k(2^k - 1)\mu^3}{(1+\mu)(2^{k-1} + (2^{k-1} - 1)\mu)(2^k + (2^k - 3)\mu)(2^k + (2^k - 1)\mu)} \tag{3.84}$$

Taking the limit of $k \to \infty$, we recover P_3^{th}.

$$\lim_{k\to\infty} \frac{(2^{k-1}-1)2^k(2^k-1)\mu^3}{(1+\mu)(2^{k-1}+(2^{k-1}-1)\mu)(2^k+(2^k-3)\mu)(2^k+(2^k-1)\mu)} = \frac{\mu^3}{(1+\mu)^4} = P_3^{th} \tag{3.85}$$

3.4.5 Coherent state incident to a Binary Tree of Beamsplitters

The coherent state in the Fock basis expansion is:

$$|\alpha\rangle = e^{-\frac{|\alpha|^2}{2}} \sum_{n=0}^{\infty} \frac{\alpha^N}{\sqrt{n!}} |n\rangle \tag{3.86}$$

So the probability of n photons is:

$$P(n) = e^{-|\alpha|^2} \frac{|\alpha|^{2n}}{n!} \tag{3.87}$$

where the mean photon number $\langle n\rangle = \mu = |\alpha|^2$. Thus, I expect to find $P(1) = e^{-|\alpha|^2}|\alpha|^2$, $P(2) = \frac{1}{2}e^{-|\alpha|^2}|\alpha|^4$, and $\frac{1}{6}e^{-|\alpha|^2}|\alpha|^6$ for large k.

When I calculate the single coincidence probability of the model,

```
Table[FullSimplify[Pmk[IdentityMatrix[2], dispVec, k, 2], {μ > 0, α > 0}], {k, 5}]
```

$$= \left\{2\, e^{-\alpha^2}\left(-1+e^{\frac{\alpha^2}{2}}\right),\ 4\, e^{-\alpha^2}\left(-1+e^{\frac{\alpha^2}{4}}\right),\ 8\, e^{-\alpha^2}\left(-1+e^{\frac{\alpha^2}{8}}\right),\ 16\, e^{-\alpha^2}\left(-1+e^{\frac{\alpha^2}{16}}\right),\ 32\, e^{-\alpha^2}\left(-1+e^{\frac{\alpha^2}{32}}\right)\right\}$$

Figure 3.14: **Single Coincidence Probability of Coherent State** for k-order trees from $k = 1$ to $k = 5$.

I can deduce the single coincidence probability for a 2N-mode beamsplitter as:

$$P(1)_k = 2^k e^{-|\alpha|^2}\left(e^{|\alpha|^2/2^k} - 1\right) \tag{3.88}$$

When I take limit of $P(1)_k$ for $k \to \infty$, I get the expected single photon probability.

$$\lim_{k\to\infty} 2^k e^{-|\alpha|^2}\left(e^{|\alpha|^2/2^k} - 1\right) = e^{-|\alpha|^2}|\alpha|^2 \tag{3.89}$$

```
Table[Simplify[Pmk2forS[IdentityMatrix[2], dispVec, TTNSymplectic[1 / Sqrt[2], k], 2], {μ > 0, α > 0}], {k, 6}]
```

$$\left\{e^{-\alpha^2}\left(-1+e^{\frac{\alpha^2}{2}}\right)^2,\ 6\, e^{-\alpha^2}\left(-1+e^{\frac{\alpha^2}{4}}\right)^2,\ 28\, e^{-\alpha^2}\left(-1+e^{\frac{\alpha^2}{8}}\right)^2,\ 120\, e^{-\alpha^2}\left(-1+e^{\frac{\alpha^2}{16}}\right)^2,\ 496\, e^{-\alpha^2}\left(-1+e^{\frac{\alpha^2}{32}}\right)^2,\ 2016\, e^{-\alpha^2}\left(-1+e^{\frac{\alpha^2}{64}}\right)^2\right\}$$

Figure 3.15: **Twofold Coincidence Probability of Coherent State** for k-order trees from $k = 1$ to $k = 6$.

I can deduce the twofold coincidence probability for a 2N-mode beamsplitter as:

$$P(2)_k = 2^{k-1}(2^k-1)e^{-|\alpha|^2}\left(e^{|\alpha|^2/2^k} - 1\right)^2 \tag{3.90}$$

When I take limit of $P(2)_k$ for $k \to \infty$, I get the expected two photon probability.

$$\lim_{k\to\infty} 2^{k-1}(2^k-1)e^{-|\alpha|^2}\left(e^{|\alpha|^2/2^k} - 1\right)^2 = \frac{1}{2}e^{-|\alpha|^2}|\alpha|^4 \tag{3.91}$$

```
Table[Simplify[Pmk3forS[IdentityMatrix[2], dispVec, TTNSymplectic[1 / Sqrt[2], k], 2], {μ > 0, α > 0}], {k, 7}]
```

$$\left\{0,\ 4-4e^{-\alpha^2}+12e^{-\frac{3\alpha^2}{4}}-12e^{-\frac{\alpha^2}{2}},\ 56e^{-\alpha^2}\left(-1+e^{\frac{\alpha^2}{8}}\right)^3,\ 560e^{-\alpha^2}\left(-1+e^{\frac{\alpha^2}{16}}\right)^3,\ 4960e^{-\alpha^2}\left(-1+e^{\frac{\alpha^2}{32}}\right)^3,\ 41\,664e^{-\alpha^2}\left(-1+e^{\frac{\alpha^2}{64}}\right)^3,\ 341\,376e^{-\alpha^2}\left(-1+e^{\frac{\alpha^2}{128}}\right)^3\right\}$$

Figure 3.16: **Threefold Coincidence Probability of Coherent State** for k-order trees from $k = 1$ to $k = 7$.

I can deduce the threefold coincidence probability for a 2N-mode beamsplitter as:

$$P(3)_k = \frac{1}{6}2^k(2^k-1)(2^k-2)e^{-|\alpha|^2}\left(e^{|\alpha|^2/2^k}-1\right)^3 \tag{3.92}$$

When I take limit of $P(3)_k$ for $k \to \infty$, I get the expected three photon probability.

$$\lim_{k\to\infty}\frac{1}{6}2^k(2^k-1)(2^k-2)e^{-|\alpha|^2}\left(e^{|\alpha|^2/2^k}-1\right)^3 = \frac{1}{6}e^{-|\alpha|^2}|\alpha|^6 \tag{3.93}$$

3.4.6 How to implement Gaussian PNR Model in Gaussian Experimental Models

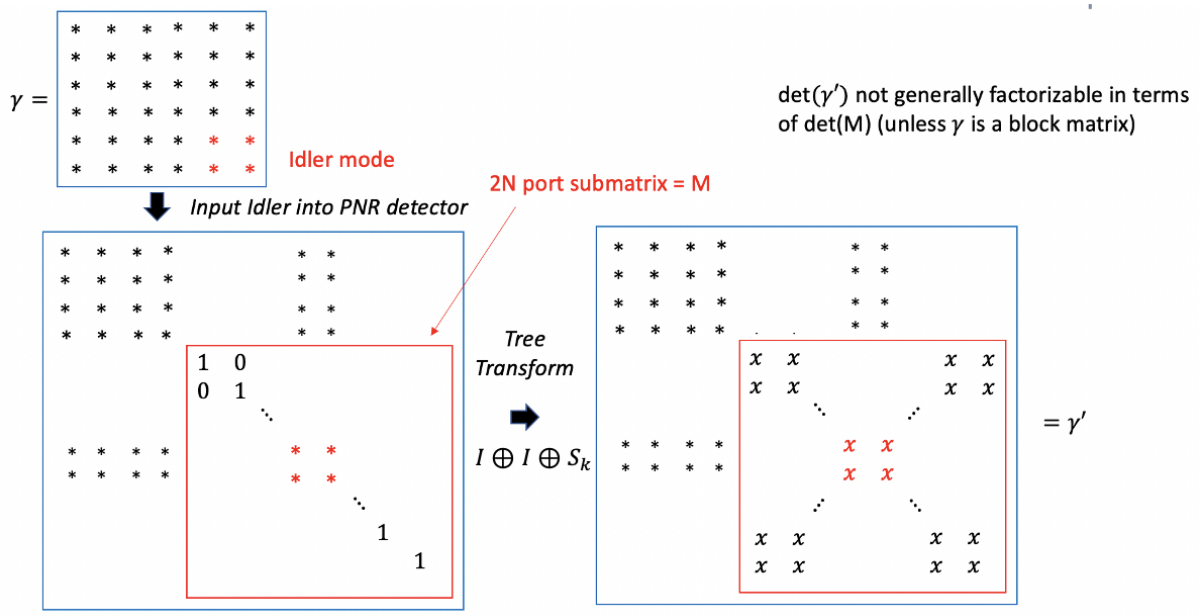

Figure 3.17: **Calculation of Threefold coincidences in $g^{(2)}(0)$ Experiment with PNR Idler in Gaussian Formalism**

3.4.7 Gaussian PNR Model for $g^2(0)$

PNR Idler Singles

$$R_{i,k} = NTr\left(\rho I_{s_1}\otimes I_{s_2}\otimes(I_m - |0\rangle\langle 0|_m)\otimes|0\rangle\langle 0|^{\otimes N-1}\right) \tag{3.94}$$

$$= NTr\left(\rho I_{s_1}\otimes I_{s_2}\otimes I_m\otimes|0\rangle\langle 0|^{\otimes N-1}\right) - NTr\left(\rho I_{s_1}\otimes I_{s_2}\otimes|0\rangle\langle 0|^{\otimes N}\right) \tag{3.95}$$

$$R_i(\mu,\eta_i,k) = \frac{2^k\mu\eta_i}{(1+\mu\eta_i)(2^k+(2^k-1)\mu\eta_i)} \tag{3.96}$$

$$\lim_{k\to\infty}R_i(\mu,\eta_i,k) = \frac{\mu\eta_i}{(1+\mu\eta_i)^2} \tag{3.97}$$

PNR Idler Signal Twofolds

$$R_{s_1,i,k} = NTr\left(\rho(I_{s_1}-|0\rangle\langle 0|_{s_1})\otimes I_{s_1}\otimes(I_m-|0\rangle\langle 0|_m)\otimes|0\rangle\langle 0|^{\otimes N-1}\right) \tag{3.98}$$

$$= NTr\left(I_{s_1} \otimes I_{s_2} \otimes I_m \otimes |0\rangle\langle 0|^{\otimes N-1}\right) - NTr\left(\rho\,|0\rangle\langle 0|_{s_1} \otimes I_{s_2} \otimes I_m \otimes |0\rangle\langle 0|^{\otimes N-1}\right) \tag{3.99}$$

$$- NTr\left(\rho I_{s_1} \otimes I_{s_2} \otimes |0\rangle\langle 0|^{\otimes N}\right) + NTr\left(\rho\,|0\rangle\langle 0|_{s_1} \otimes I_{s_2} \otimes |0\rangle\langle 0|^{\otimes N}\right) \tag{3.100}$$

$$R_{is_j}(\mu,\eta_i,\eta_{sj},k) = 2^k\Bigg(\frac{1}{-1-\mu\eta_i} + \frac{2^k}{2^k+(2^k-1)\mu\eta_i} \tag{3.101}$$

$$+ \frac{2}{2+2\mu\eta_i+\eta_{sj}\mu(1-\eta_i)} - \frac{2^{k+1}}{\mu\eta_{sj}(2^k-(2^k-1)\eta_i)+2(2^k+(2^k-1)\mu\eta_i)}\Bigg) \tag{3.102}$$

$$\lim_{k\to\infty} R_{is_j}(\mu,\eta_i,\eta_{s1},k) = \mu\eta_i\left(\frac{1}{(1+\mu\eta_i)^2} + \frac{2\,(-2+\eta_{sj})}{(\mu\eta_{sj}\,(-1+\eta_i)-2\,(1+\mu\eta_i))^2}\right) \tag{3.103}$$

PNR Idler Threefolds $N = 2^k$

$$R_{s_1,s_2,i,k} = NTr\left(\rho I_{s_1} - |0\rangle\langle 0|_{s_1}) \otimes (I_{s_1} - |0\rangle\langle 0|_{s_1}) \otimes (I_m - |0\rangle\langle 0|_m) \otimes |0\rangle\langle 0|^{\otimes N-1}\right) \tag{3.104}$$

$$= NTr\left(\rho I_{s_1} \otimes I_{s_2} \otimes I_m \otimes |0\rangle\langle 0|^{\otimes N-1}\right) - NTr\left(\rho\,|0\rangle\langle 0|_{s_1} \otimes I_{s_2} \otimes I_m \otimes |0\rangle\langle 0|^{\otimes N-1}\right) \tag{3.105}$$

$$- NTr\left(\rho I_{s_1} \otimes |0\rangle\langle 0|_{s_2} \otimes I_m \otimes |0\rangle\langle 0|^{\otimes N-1}\right) + NTr\left(\rho\,|0\rangle\langle 0|_{s_1} \otimes |0\rangle\langle 0|_{s_2} \otimes I_m \otimes |0\rangle\langle 0|^{\otimes N-1}\right) \tag{3.106}$$

$$- NTr\left(\rho I_{s_1} \otimes I_{s_2} \otimes |0\rangle\langle 0|^{\otimes N}\right) + NTr\left(\rho\,|0\rangle\langle 0|_{s_1} \otimes I_{s_2} \otimes |0\rangle\langle 0|^{\otimes N}\right) \tag{3.107}$$

$$+ NTr\left(\rho I_{s_1} \otimes |0\rangle\langle 0|_{s_2} \otimes |0\rangle\langle 0|^{\otimes N}\right) - NTr\left(\rho\,|0\rangle\langle 0|_{s_1} \otimes |0\rangle\langle 0|_{s_2} \otimes |0\rangle\langle 0|^{\otimes N}\right) \tag{3.108}$$

$$R_{i,s_1,s_2}(\mu,\eta_{s_1},\eta_{s_2},\eta_i,k) = 2^k\Bigg(-\frac{1}{1+\mu\eta_i} + \frac{2^k}{2^k+(2^k-1)\,\mu\eta_i} + \frac{2}{2+2\mu\eta_i+\eta_{s1}\,(\mu-\mu\eta_i)} \tag{3.109}$$

$$+ \frac{2}{2+2\mu\eta_i+\eta_{s2}\,(\mu-\mu\eta_i)} - \frac{2}{2+2\mu\eta_i+\eta_{s1}\,(\mu-\mu\eta_i)+\eta_{s2}\,(\mu-\mu\eta_i)} \tag{3.110}$$

$$- \frac{2^{k+1}}{\mu\eta_{s1}\,(2^k-(2^k-1)\,\eta_i)+2\,(2^k+(2^k-1)\,\mu\eta_i)} \tag{3.111}$$

$$- \frac{2^{k+1}}{\mu\eta_{s2}\,(2^k-(2^k-1)\,\eta_i)+2\,(2^k+(2^k-1)\,\mu\eta_i)} \tag{3.112}$$

$$+ \frac{2^{k+1}}{\mu\eta_{s1}\,(2^k-(2^k-1)\,\eta_i)+\mu\eta_{s2}\,(2^k-(2^k-1)\,\eta_i)+2\,(2^k+(2^k-1)\,\mu\eta_i)}\Bigg) \tag{3.113}$$

$$\lim_{k\to\infty} R_{i,s_1,s_2}(\mu,\eta_{s_1},\eta_{s_2},\eta_i,k) = \mu\eta_i\Bigg(\frac{1}{(1+\mu\eta_i)^2} + \frac{2\,(-2+\eta_{s_1})}{(\mu\eta_{s_1}\,(-1+\eta_i)-2\,(1+\mu\eta_i))^2} \tag{3.114}$$

$$+ \frac{2\,(-2+\eta_{s_2})}{(\mu\eta_{s_2}\,(-1+\eta_i)-2\,(1+\mu\eta_i))^2} - \frac{2\,(-2+\eta_{s_1}+\eta_{s_2})}{(\mu\eta_{s_1}\,(-1+\eta_i)\,\mu\eta_{s_2}\,(-1+\eta_i)-2\,(1+\mu\eta_i))^2}\Bigg) \tag{3.115}$$

Introducing Thermal Modes

$$\mathrm{Tr}\left(\rho I_{s_1} \otimes I_{s_2} \otimes I_m \otimes |0\rangle\left\langle 0|^{\otimes N-1}\right.\right) = \frac{2^k}{2^k+(2^k-1)\mu\eta_i} \tag{3.116}$$

$$\mathrm{Tr}\left(\rho|0\rangle\left\langle 0|_{s_1} \otimes I_{s_2} \otimes I_m \otimes \right| 0\right\rangle\left\langle 0|^{\otimes N-1}\right.\right) = \frac{2^{k+1}}{\mu\eta_{s_1}\,(2^k-(2^k-1)\eta_i)+2\,(2^k+(2^k-1)\mu\eta_i)} \tag{3.117}$$

$$\mathrm{Tr}\left(\rho I_{s_1} \otimes |0\rangle\left\langle 0|_{s_2} \otimes I_m \otimes \right| 0\right\rangle\left\langle 0|^{\otimes N-1}\right.\right) = \frac{2^{k+1}}{\mu\eta_{s_2}\,(2^k-(2^k-1)\eta_i)+2\,(2^k+(2^k-1)\mu\eta_i)} \tag{3.118}$$

$$\mathrm{Tr}\left(\rho|0\rangle\langle 0|_{s_1}\otimes|0\rangle\langle 0|_{s_2}\otimes I_m\otimes|0\rangle\left\langle 0|^{\otimes N-1}\right.\right)=\frac{2^{k+1}}{\mu(\eta_{s_1}+\eta_{s_2})(2^k-(2^k-1)\eta_i)+2(2^k+(2^k-1)\mu\eta_i)} \tag{3.119}$$

$$\mathrm{Tr}\left(\rho I_{s_1}\otimes I_{s_2}\otimes|0\rangle\left\langle 0|^{\otimes N}\right.\right)=\frac{1}{1+\mu\eta_i} \tag{3.120}$$

$$\mathrm{Tr}\left(\rho|0\rangle\langle 0|_{s_1}\otimes I_{s_2}\otimes|0\rangle\left\langle 0|^{\otimes N}\right.\right)=\frac{2}{2+2\mu\eta_i+\eta_{s_1}\mu(1-\eta_i)} \tag{3.121}$$

$$\mathrm{Tr}\left(\rho I_{s_1}\otimes|0\rangle\langle 0|_{s_2}\otimes|0\rangle\left\langle 0|^{\otimes N}\right.\right)=\frac{2}{2+2\mu\eta_i+\eta_{s_2}\mu(1-\eta_i)} \tag{3.122}$$

$$\mathrm{Tr}\left(\rho|0\rangle\langle 0|_{s_1}\otimes|0\rangle\langle 0|_{s_2}\otimes|0\rangle\left\langle 0|^{\otimes N}\right.\right)=\frac{2}{2+2\mu\eta_i+(\eta_{s_1}+\eta_{s_2})\mu(1-\eta_i)} \tag{3.123}$$

3.4.8 Extensions of PNR Gaussian Modeling: Beamsplitter Tensor Networks as Quantum Circuits

Are there other tensor networks that are more computationally efficient, i.e. distribute photons more efficiently over output modes?

Some complexity considerations include the number of layers and the depth of layers. For TTN, to

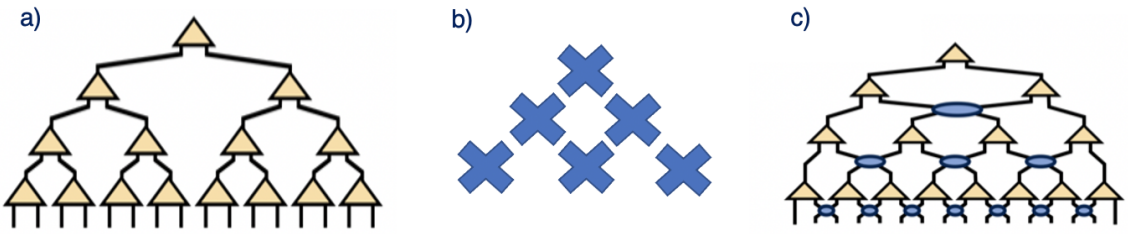

Figure 3.18: **Complexity Considerations** a) Binary TTN b) "Mesh" lattice (Quantum random walk) c) MERA

reach large k, we need a small number of layers, but each layer has large depth.

Can we use a network that has a better trade off between number of layers and depth of layers to simulate a large k circuit with less complexity? We might consider next a mesh lattice of beamsplitters. This would require a large number of layers, but each layer low depth. However, the semiclassical picture breaks down since there is interference between photons (not just vacuum modes as in the TTN) at each layer. We can recognize this as a quantum random walk (or boson sampling), which sends the photons to the left and right extremities.

Next we can consider something in between the TTN and the mesh lattice, where for each layer we sandwich a mesh layer between slices of the TTN. This looks a lot like the multi-scale entanglement renormalization ansatz (MERA), which is a quantum circuit that has been proposed for efficient simulation of complex N-body systems [17].

A MERA is a tensor network M that corresponds to the quantum circuit C, where each two-body unitary gate of C gives rise to a tensor of M. In the tensor network, incoming wires in state $|0\rangle$ are eliminated, producing three kinds of tensors: (i) the top tensor $t = u\,|0\rangle\,|0\rangle$,

$$(t)_{\mu\nu}=(u)^{\alpha\beta}_{\mu\nu}\big|_{\alpha,\beta=0} \qquad \sum_{\mu\nu}(t^*)_{\mu\nu}(t)_{\mu\nu}=1 \tag{3.124}$$

(ii) tensors in every second row are isometries $w = u\,|0\rangle$,

$$(w)^{\alpha}_{\mu\nu}=(u)^{\alpha\beta}_{\mu\nu}\big|_{\alpha=0} \qquad \sum_{\mu\nu}(w^*)^{\alpha}_{\mu\nu}(w)^{\alpha'}_{\mu\nu}=\delta_{\alpha\alpha'} \tag{3.125}$$

and (iii) the rest of the tensors in M are unitary gates u (aka disentanglers),

$$\sum_{\mu\nu}(u^*)^{\alpha\beta}_{\mu\nu}(u)^{\alpha'\beta'}_{\mu\nu}=\delta_{\alpha\alpha'}\delta_{\beta\beta'} \tag{3.126}$$

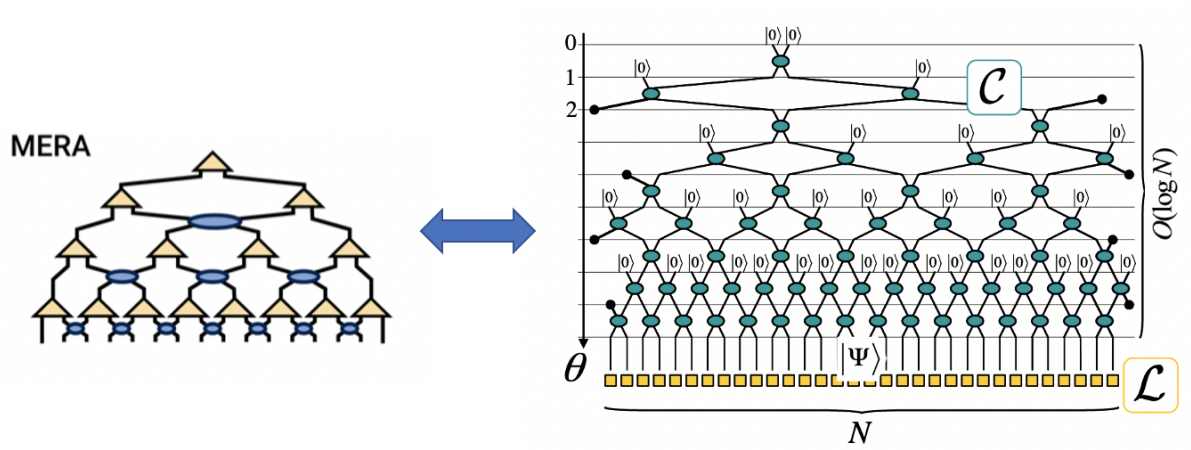

FIG. 1: Quantum circuit $\mathcal{C}$ transforms state $|0\rangle^{\otimes N}$ into the N-site state $|\Psi\rangle$ of a 1D lattice $\mathcal{L}$. $\mathcal{C}$ contains $2N-1$ gates organized in $O(\log N)$ layers labeled by a discrete time θ.

Figure 3.19: **Multi-scale entanglement renormalization ansatz (MERA)**

$$\sum_{\alpha\beta}(u^*)^{\alpha\beta}_{\mu\nu}(u)^{\alpha\beta}_{\mu'\nu'} = \delta_{\mu\mu'}\delta_{\nu\nu'} \tag{3.127}$$

The computational space required to store M grows linearly in N as $O(\chi^4 N)$, since there are $2N-1$ tensors and each tensor depends on at most χ^4 parameters [17].

MERA in Gaussian Formalism

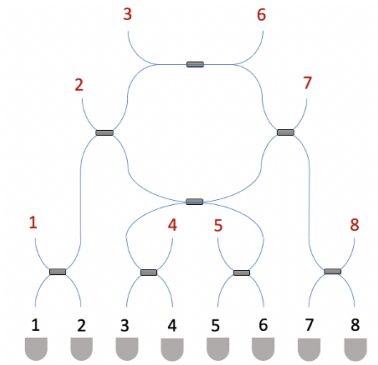

Figure 3.20: MERA as beamsplitter network

I am modeling a MERA as layers of a binary TTN alternated with a "mesh" layer.

Extensions

- Could tensor network circuits for efficiently creating complex N-body states be useful on photonic platform?
  - Error correction using cluster states
  - Photonic quantum memory?
  - All-photonic quantum repeater [4] [10] [18]
- Could we use MERA as an ansatz for cluster states on quantum photonic platform?
  - Perform classical simulation for QML to learn optimal weights for experiment
- Could we realize quantum photonic on-chip tensor networks for experimental QML demonstration?
  - Non-barren plateau for TTN [22]. Work out theory for MERA?
  - Quantum convolutional neural network
- Classically simulate QML for experimental design of tensor network circuit for quantum network
- Hybrid QML on fiber optic quantum network
  - Perform QML using remote feedback on CQNET
- Could we use quantum photonic tensor network circuits like MERA for quantum supremacy?
  - Has quantum supremacy been demonstrated on a photonic platform (e.g. on chip)?
- Could we use quantum photonic tensor network circuits like MERA for quantum simulation of N-body states for e.g. probing condensed matter and high energy physics?